

Broad transcriptional dysregulation of brain and choroid plexus cell types with COVID-19

Andrew C. Yang^{1,2,3,#}, Fabian Kern^{4,#}, Patricia M. Losada³, Christina A. Maat³, Georges Schmartz⁴, Tobias Fehlmann⁴, Nicholas Schaum³, Davis P. Lee³, Kruti Calcuttawala³, Ryan T. Vest³, David Gate³, Daniela Berdnik³, M. Windy McNerney⁵, Divya Channappa³, Inma Cobos^{3,6}, Nicole Ludwig⁷, Walter J. Schulz-Schaeffer⁸, Andreas Keller^{3,4,*}, Tony Wyss-Coray^{2,3,9,10,*}

1 Department of Bioengineering, Stanford University School of Medicine, Stanford, California, USA.

2 ChEM-H, Stanford University, Stanford, California, USA.

3 Department of Neurology and Neurological Sciences, Stanford University School of Medicine, Stanford, California, USA.

4 Chair for Clinical Bioinformatics, Saarland University, 66123 Saarbrücken, SL, Germany.

5 Department of Psychiatry, Stanford University School of Medicine, Stanford, California, USA.

6 Department of Pathology, Stanford University School of Medicine, Stanford, California, USA.

7 Department of Human Genetics, Saarland University, 66421 Homburg/Saar, Germany.

8 Institute for Neuropathology, Saarland University Hospital and Medical Faculty of Saarland University.

9 Wu Tsai Neurosciences Institute, Stanford University, Stanford, CA, USA.

10 Paul F. Glenn Center for the Biology of Aging, Stanford University School of Medicine, Stanford, California, USA.

These authors contributed equally

* Correspondence to andreas.keller@ccb.uni-saarland.de or twc@stanford.edu

1 Abstract

2 Though SARS-CoV-2 primarily targets the respiratory system, it is increasingly
3 appreciated that patients may suffer neurological symptoms of varied severity^{1–3}. However, an
4 unbiased understanding of the molecular processes across brain cell types that could contribute
5 to these symptoms in COVID-19 patients is still missing. Here, we profile 47,678 droplet-based
6 single-nucleus transcriptomes from the frontal cortex and choroid plexus across 10 non-viral, 4
7 COVID-19, and 1 influenza patient. We complement transcriptomic data with
8 immunohistochemical staining for the presence of SARS-CoV-2. We find that all major cortex
9 parenchymal and choroid plexus cell types are affected transcriptionally with COVID-19. This
10 arises, in part, from SARS-CoV-2 infection of the cortical brain vasculature, meninges, and
11 choroid plexus, stimulating increased inflammatory signaling into the brain. In parallel,
12 peripheral immune cells infiltrate the brain, microglia activate programs mediating the
13 phagocytosis of live neurons, and astrocytes dysregulate genes involved in neurotransmitter
14 homeostasis. Among neurons, layer 2/3 excitatory neurons—evolutionarily expanded in
15 humans⁴—show a specific downregulation of genes encoding major SNARE and synaptic
16 vesicle components, predicting compromised synaptic transmission. These perturbations are
17 not observed in terminal influenza. Many COVID-19 gene expression changes are shared with
18 those in chronic brain disorders and reside in genetic variants associated with cognitive
19 function, schizophrenia, and depression. Our findings and public dataset provide a molecular
20 framework and new opportunities to understand COVID-19 related neurological disease.

21

22 Main Text

23 Severe Acute Respiratory Syndrome Coronavirus 2 (SARS-CoV-2), the etiologic agent
24 of the COVID-19 global pandemic, has as of October 2020 infected over 40 million people and

25 caused over a million deaths worldwide (worldometers.info/coronavirus). Though SARS-CoV-2
26 primarily targets the respiratory system, it is increasingly appreciated that COVID-19 patients
27 can suffer neurological and psychiatric symptoms of varied severity, depending on SARS-CoV-2
28 mechanisms as well as other variables, such as co-morbidities and clinical care^{1–3,5}. Central
29 nervous system (CNS) symptoms range from loss of smell and headache to memory loss,
30 encephalitis, stroke, difficulty concentrating, and persistent fatigue^{1,6–8}. Symptoms are especially
31 frequent and prominent in the over 20% of COVID-19 patients that require hospitalization^{1,9–11}.
32 With lingering CNS symptoms documented in Severe Acute Respiratory Syndrome (SARS) and
33 Middle East Respiratory Syndrome (MERS) survivors^{1,12–14}, it remains to be seen whether such
34 chronic symptoms will emerge in COVID-19 survivors.

35 Cellular and molecular approaches are required to understand the neurological changes
36 that may contribute to symptoms reported in COVID-19 patients. Fundamentally, pathology can
37 arise from the direct infection of neurons and glia or indirectly from peripheral infection and its
38 attendant immune response^{15,16}. Viral RNA has been detected in the olfactory mucosa and
39 cerebrospinal fluid (CSF) in some cases, but the consequences for brain cells remain unclear^{17–}
40 ²⁰. Several reports using elegant *in vitro* culture systems, such as neuronal organoids, have
41 reached conflicting conclusions regarding the potential for SARS-CoV-2 neuroinvasion^{21–26}. The
42 physiological relevance of such cultured systems, from the viral titers applied to their fidelity to
43 actual patient brains, also remains unclear^{23,27,28}. Missing so far is an unbiased view of the
44 molecular and cellular perturbations across brain cell types in COVID-19 patients. This is in part
45 because high-quality human brain tissue from patients for such studies is largely
46 inaccessible^{21,23,24}. Furthermore, several brain regions highly relevant to COVID-19, such as the
47 choroid plexus^{23,24}, have not yet been successfully profiled in humans at single-cell resolution, in
48 health or disease²⁹.

49 Here, we profile 47,678 droplet-based single-nucleus transcriptomes from the frontal
50 cortex and choroid plexus across 10 non-viral, 4 COVID-19, and 1 influenza patient (Fig. 1a).
51 We complement transcriptomic data with immunohistochemical staining for the presence of
52 SARS-CoV-2. These data—which includes the first, to our knowledge, single-cell view of
53 neurological changes in COVID-19 and of the human choroid plexus in general—provide a
54 molecular framework for how SARS-CoV-2 affects the brain without requiring direct
55 neuroinvasion; reveals the major pathways and cell types perturbed; and highlights associations
56 with chronic CNS diseases potentially pertinent to COVID-19 survivors. We created an
57 interactive data browser (https://tvc-stanford.shinyapps.io/scRNA_Brain_COVID19), which will

58 be updated as more patient samples become available, to provide a resource for researchers to
59 further dissect the molecular mechanisms of SARS-CoV-2's impacts on the brain.
60

61 **Cell type-specific gene expression changes in the COVID-19 brain**

62 We aimed to gain insight into the cell type–specific transcriptomic effects of COVID-19
63 on the brain by performing unbiased single-nucleus RNA sequencing (snRNA-seq) of 15 fresh-
64 frozen postmortem medial frontal cortex and lateral ventricle choroid plexus samples from 10
65 non-viral, 4 COVID-19, and 1 influenza patient of similar clinical course as the COVID-19
66 patients (Extended Data Table 1). Our sample sizes were similar to those reported in previous
67 snRNA-seq studies^{30–32}. Samples in the control and COVID-19 groups were between 58 and 91
68 years old and matched for tissue dissection area and RNA quality (Extended Data Fig. 1,
69 Extended Data Table 1). Cause of death for COVID-19 and influenza patients was consistently
70 interstitial pneumonia after more than two weeks of mechanical ventilation. Two COVID-19
71 patients experienced objective neurological symptoms during care (Extended Data Table 1).
72 Samples were not confounded by technical or batch artifacts (Extended Data Fig. 2).

73 To begin, we generated 23,626 single-nuclei gene expression profiles from the medial
74 frontal cortex (4 non-viral, 4 COVID-19, 1 influenza)—and detected a median of 1,486 genes
75 per nucleus, a yield that is in line with recent snRNA-seq studies (Fig. 1b, Extended Data Fig.
76 1)^{31–34}. We performed unbiased clustering of nuclear profiles to identify and annotate 8 cell
77 types, including subtypes of excitatory neurons and interneurons. Each annotated cell type
78 expressed previously established marker genes (Extended Data Fig. 3): excitatory neurons
79 (e.g., marked by *CBLN2* and *NRGN*), inhibitory neurons (*GAD1*), astrocytes (*AQP4*),
80 oligodendrocytes (*MBP* and *ST18*), microglia (*DOCK8*), oligodendrocyte progenitor cells
81 (*VCAN*), maturing neurons (*DACH1*), and endothelial cells (*LEPR*)—though this latter
82 population also contains mixed markers for vascular mural pericytes and smooth muscle cells,
83 as in prior reports^{32,34,35}. Overall, the cell type identities, markers, and proportions match prior
84 snRNA-seq data from adult human cortex (Extended data Fig. 1–4, Extended Data Table 2)^{31–34}.

85 We compared levels of gene expression in cells isolated from COVID-19 versus non-
86 viral control individuals by cell type and identified 2,194 unique differentially expressed genes
87 (DEGs) that implicated all major cell types (Extended Data Table 3). As recently reported in
88 Alzheimer's disease (AD)³⁴, neurons exhibited a strong signature of repression—73% of DEGs
89 in excitatory neurons and 65% in interneurons were downregulated—whereas DEGs in glial
90 oligodendrocytes, OPCs, astrocytes, and microglia were more balanced (36–51%, Fig. 1c-d).
91 The number of DEGs was greatest for astrocytes, excitatory neurons, and oligodendrocytes,

92 partially reflecting increased power in these higher-abundance cell types. The vast majority of
93 DEGs were perturbed in only a single cell type (~84%, Fig. 1e-f, Extended Data Fig. 5a), further
94 indicating a cell type-specific CNS response to COVID-19. However, the minority of shared
95 DEGs clustered into meaningful pathways: for example, commonly downregulated DEGs
96 implicated impairments in brain-derived neurotrophic factor (BDNF) and interleukin-2 (IL-2)
97 signaling (Fig. 1f), both critical for homeostatic neuronal function^{36–40}. Overall, these results
98 indicate that all major brain parenchymal cell types are affected at the transcriptional level by
99 COVID-19, and that single-cell-level resolution is critical because changes in gene expression—
100 including directionality—are dependent on cell type.

101

102 **SARS-CoV-2 accumulation in barrier cells stimulates inflammatory signaling to the brain**

103 The observed transcriptional response to COVID-19 in the brain could arise from direct
104 neurotropism or indirect damage via peripheral inflammation^{15,16}. We thus stained for the SARS-
105 CoV-2 spike glycoprotein^{20,41} in medial frontal cortex and choroid plexus tissue immediately
106 adjacent to tissue used in snRNA-seq. Intriguingly, we detected spike glycoprotein robustly in
107 two COVID-19 patients (Fig. 2). Upon closer examination however, spike glycoprotein signal
108 resided only within the barrier-forming cortical vasculature, meninges, and choroid plexus.
109 Within the choroid plexus, signal appeared within the stromal compartment, though confident
110 cell type assignment was not possible (Fig. 2c). Thus, unlike recent reports where SARS-CoV-2
111 was added directly to neuroglial organoids lacking brain-barrier cells^{21–25}, we do not observe
112 significant virus invasion in cortex parenchymal cells. On the other hand, SARS-CoV-2 infection
113 of the CSF-barrier forming choroid plexus and meninges corroborates recent *in vitro*, *in silico*,
114 CSF, and postmortem case studies suggesting CNS barrier cells can support productive
115 infection at relatively low titers^{5,23,24,42,43}. We note however that this absence of detectable
116 SARS-CoV-2 neuroinvasion does not exclude its possibility. Likewise, it is possible that the
117 other two COVID-19 patients sustain SARS-CoV-2 barrier cell infection undetected in the tissue
118 sampled. Corroborating a recent study⁵, presence of SARS-CoV-2 in the CNS did not correlate
119 with neurological symptoms (Extended Data Table 1). Together, these results suggest that
120 brain-barrier cells may be particularly susceptible to SARS-CoV-2 infection, and that preferential
121 accumulation of virus in the barriers may give rise to widespread cortical DEGs.

122 Because we detected SARS-CoV-2 spike glycoprotein in the blood-brain and blood-
123 CSF-barrier cells, we sought to devise methods to profile these cells and better understand their
124 relation to cortical transcriptional perturbations with COVID-19. However, conventional brain
125 snRNA-seq preparation methods nearly universally deplete high-quality brain vascular nuclei

126 from endothelial cells, pericytes, smooth muscle cells, and fibroblasts for currently unknown
127 reasons^{32–35}. At the same time, no snRNA-seq study exists on the human choroid plexus, in
128 health or disease. This could, as we discovered, be because enzymatic and dounce
129 homogenization techniques successfully used to process mouse tissue²⁹ resulted in a near
130 complete loss of genes in isolated human choroid nuclei. We thus generated a method involving
131 successive gentle triturations in mild detergent (Methods), yielding 24,052 nuclei across 7 major
132 epithelial, mesenchymal, immune, and glial cell types (6 non-viral, 4 COVID-19, 1 influenza; Fig.
133 3a, Extended Data Fig. 4, Extended Data Table 4).

134 Epithelial cells accounted for 81% of choroid nuclei profiled, and interestingly,
135 subclustered based on expression of the receptor (PRLR) for prolactin—a hormone mediating
136 neurogenesis^{44,45}, the glutathione peroxidase GPX3—which protects the CSF from
137 hydroperoxides⁴⁶, and the chloride anion exchanger SLC26A3—which may maintain
138 physiologic ion concentrations in the CSF⁴⁷. Similar to brain vascular cells^{16,48}, the choroid
139 barrier and stromal epithelial, endothelial, mesenchymal, and ependymal cells robustly
140 expressed the antiviral defense gene *IFITM3*. Intriguingly, we observed a broad upregulation of
141 *IFITM3* across barrier cells in COVID-19 patients, consistent with immunohistochemical
142 detection of SARS-CoV-2 infection (Fig. 3b). *IFITM3* serves as the first line of defense against
143 viral infection⁴⁹ and its upregulation is a marker of SARS-CoV-2 infection across publicly
144 available datasets⁵⁰. We also observed in the cortex parenchyma a consistent upregulation of
145 the newly described viral entry receptor *NRP1*^{41,51,52} (Fig. 3b, Extended Data Fig. 6), which has
146 been previously found upregulated in inflamed COVID-19 lung tissue^{51,53}.

147 Overall, the DEGs detected in choroid epithelial cells, mesenchymal cells, and
148 monocytes indicate strong CNS inflammation in COVID-19 (Fig. 3c-e, Extended Data Table 5).
149 For example, we observed upregulation of the pro-inflammatory cytokine IL-1 β , which has been
150 reported sufficient to induce pathologic microglial and astrocyte activation^{54,55}. The coincident
151 upregulation of *IL-1 β* , *CCL2*, and *CCL4* further suggests a weakened choroid barrier and an
152 increasingly permissive environment for immune cell transmigration into the brain
153 parenchyma^{56–58}. The aged choroid plexus has recently been reported to send inflammatory
154 signals to the brain, thereby activating glia and impairing cognitive function^{59,60}. To assess if
155 similar pro-inflammatory signaling mechanisms occur in COVID-19, we performed cell-cell
156 communication analysis^{61,62}. We observed a strong increase in choroid-to-cortex signaling
157 across key inflammatory pathways, such as the CCL and CXCL family of chemokines (Fig. 3f,
158 Extended Data Fig. 5b). Together, these results suggest that SARS-CoV-2 can infect and

159 inflame brain-barrier cells, including the choroid plexus; and that this barrier—together with
160 peripheral—inflammation is then relayed into the brain parenchyma.
161

162 **Immune cell infiltration and activation of neuronal engulfment programs in microglia**

163 We sought to evaluate the predicted activation of brain microglia and migration of
164 peripheral immune cells via enhanced inflammatory signaling from the periphery and brain-
165 barrier cells. Intriguingly, we observed in the cortex a COVID-19 enriched subpopulation of
166 microglia (Fig. 4a-b, Extended Data Fig. 7-8). This cluster was marked by expression of genes
167 implicated in human microglial activation, such as *CD74*, *FTL*, and *FTH1* (Extended Data Table
168 6). These very genes have recently been described as difficult to detect by snRNA-seq⁶³, further
169 underscoring strong COVID-19 microglial activation. An over-represented fraction of COVID-19
170 microglia cluster marker genes overlap ($P < 10^{-25}$, hypergeometric test) with human Alzheimer's
171 disease microglia cluster markers³⁴ (Extended Data Fig. 7c). Monocle trajectory analysis⁶⁴ found
172 that the COVID-19 microglia cluster emerged from the parent homeostatic population—and that
173 the expression of activation markers increased along the pseudotime route—, suggesting that
174 these microglia emerged in response to an increasingly inflamed CNS environment (Fig. 4c,
175 Extended Data Fig. 7a-b), consistent with enhanced brain-barrier inflammatory signaling. Our
176 observations suggest that the COVID-19 subpopulation represents a distinct microglial state
177 that shares features with, but is ultimately different from, microglial cell states previously
178 reported in human neurodegenerative disease.

179 We next assessed the predicted increase in peripheral immune cell infiltration. We
180 indeed found both an increase in T-cells (marked by *CD247* encoding the TCR CD3-zeta
181 protein, Fig. 4d, Extended Data Fig. 8e) and an increase in peripheral macrophages (marked by
182 *F13A1*^{65,66}, Fig. 4e). Microglial activation and enhanced immune cell infiltration have been
183 recently reported by IHC staining in a series of 43 COVID-19 brains, with the degree of
184 infiltration and glial activation not clearly correlated with neurological symptoms or the presence
185 of detectable virus in the brain⁵. Our results largely corroborate those findings via an orthogonal
186 snRNA-seq approach (Fig. 4a-e). Both the formation of a distinct microglial cluster and the
187 enhanced infiltration of peripheral T-cells and macrophages did not occur in terminal influenza,
188 suggesting a COVID-19 specific—or at least not a pan-viral—CNS response.

189 Because we collected sufficient microglia for DEG analysis, we sought a clearer
190 understanding of the functional ramifications of their COVID-19 activation. As expected,
191 established markers of microglial activation previously linked to pathologic functions such as
192 *CD74* and *MERTK* were strongly upregulated⁶⁷⁻⁷⁴. We observed a concomitant loss of the

193 immune checkpoint molecules *MEF2C* and *IRAK3* that restrain runaway inflammation^{75–77}.
194 Recently, increased microglial phagocytosis of live neurons—termed phagoptosis—has been
195 demonstrated to be an important mechanism driving various neurodegenerative diseases^{71,78–81}.
196 Remarkably, nearly every gene reported⁸¹ to mediate microglial phagocytosis of live neurons is
197 strongly upregulated in COVID-19 microglia (Fig. 4g). These include the genes encoding
198 complement proteins C3, all three components of C1Q, and the pro-phagocytic receptors
199 MERTK and VNR. Together, these data reveal in the COVID-19 brain the infiltration of immune
200 cells and strong activation of a pathologic microglial phagocytosis program predicted to
201 prematurely engulf and prune live neurons.
202

203 **Potential synaptic dysfunction specifically in layer 2/3 excitatory neurons**

204 The global induction of microglial phagoptosis programs prompted us to look into other
205 potential signatures of neuronal compromise. Astrocytes play a dual role in both forming the glia
206 limitans barrier^{82,83} and supporting homeostatic neuronal function^{84–86} (Fig. 5a). Given SARS-
207 CoV-2 infection of barrier cells, we thus wondered whether astrocytes would exhibit similar
208 hallmarks of inflammation with concomitant consequences for neuronal health. We indeed
209 observed hallmarks of astrogliosis⁸⁷ and viral defense⁵⁰ in upregulated *GFAP* and *IFITM3*
210 expression, as well as neurotoxicity in the secreted factor CHI3L1^{88–90} (Fig. 3b, Fig. 5a-d).
211 Forming a tripartite synapse with neurons, astrocytes finely balance the levels of synaptic
212 neurotransmitters like glutamate via the dedicated transporters EEAT1 (*SLC1A3*) and EEAT2
213 (*SLC1A2*)^{91–93}. Dysregulated glutamate transporter expression causes neuronal dysfunction:
214 downregulation results in excess glutamate excitotoxicity^{94,95} and extrasynaptic spillover^{96,97};
215 whereas upregulation impairs long-term potentiation (LTP) and synaptic plasticity^{98–101}. We
216 observed dysregulated overexpression of genes predicting diminished glutamate signaling
217 across synapses: for example, the overexpression of both glutamate transporters (*SLC1A2* and
218 *SLC1A3*, Fig. 5a, e) as well as the major potassium uptake channel Kir4.1 (*KCNJ10*), which
219 reduces neuronal excitability by lowering extracellular potassium, glutamate, and BDNF¹⁰².

220 We next sought to identify the neuronal subtypes affected in COVID-19. Enrichment
221 analysis implicated potential impairments in synaptic transmission specifically in excitatory
222 neurons (Extended Data Fig. 9). Among COVID-19 patients, those with objective neurological
223 symptoms or detectable virus did not exhibit further deficits in the expression of genes
224 mediating synaptic transmission (Extended Data Fig. 9c, Extended Data Table 1). Glutamate
225 release at synapses is critical for fast and faithful communication between neurons for
226 information processing in sub-second timeframes^{103–105}. Glutamate is stored in readily

227 releasable pools of vesicles within presynaptic terminals. During synaptic transmission, SNARE
228 proteins play an indispensable role in vesicle docking, priming, fusion, and synchronization of
229 glutamate release into the synaptic cleft^{103,104}. Downregulation of the mRNA encoding SNARE
230 components has been found in various neurological diseases^{106–109}, and is sufficient in
231 experimental models to impair both vesicle processing and overall neuronal viability^{110–114}. We
232 observed in COVID-19 excitatory neurons a consistent downregulation of major SNARE
233 components (Fig. 5f). For example, genes encoding both v-SNARE synaptobrevins (*VAMP1*,
234 *VAMP2*) necessary for calcium-dependent glutamate release^{115,116} decreased. Likewise,
235 expression diminished for the partner t-SNARE proteins syntaxin 1B (*STX1B*) and SNAP-25,
236 also necessary^{117,118} for glutamate release.

237 The human neocortex is composed of six layers of interconnected excitatory and
238 inhibitory neurons, with each layer both highly specialized locally and integrated globally. Of
239 these six layers, layers 2 and 3 are disproportionately thickened during the evolution of the
240 human brain, playing a key role in higher brain functions such as cognition, learning, memory,
241 creativity, and abstraction^{4,119,120}. Though we captured neurons from all cortical layers, we found
242 that gene expression changes linked to synaptic deficits are specific to only these layer 2/3
243 excitatory neurons (Fig. 5g). L2/3 excitatory neurons already exhibit sparse action potential
244 firing to generate a simple and reliable neural code for associative learning¹²⁰. Thus, this
245 neuronal population may be particularly sensitive to the predicted deficits in neurotransmission
246 with COVID-19. Together, these data suggest potential impairments in L2/3 neuron synaptic
247 transmission, plasticity, and LTP in COVID-19, due to the dysregulation of genes mediating
248 astrocyte glutamate homeostasis and genes encoding major synaptic vesicle components.
249

250 **Associations with chronic CNS disease**

251 Reports of lingering CNS complications in COVID-19 survivors are emerging¹²¹. To
252 provide a molecular rationale for these complications, we compared COVID-19 cell type-specific
253 DEGs with those recently described by snRNA-seq in chronic CNS diseases, including
254 Alzheimer's disease³⁴, multiple sclerosis¹²², Huntington's disease¹²³, and autism spectrum
255 disorder³³. Surprisingly, the overlap of DEGs between COVID-19 and these chronic CNS
256 diseases was over-represented for each cell type (Fig. 6a, Extended Data Fig. 10, Extended
257 Data Table 7). The degree of overlap was particularly high in astrocytes and excitatory neurons.
258 For example, genes encoding the SNARE protein SNAP-25 and the neurotrophic factor BDNF
259 were commonly downregulated in excitatory neurons in both COVID-19 and Alzheimer's

260 disease³⁴. This over-representation of overlapping DEGs suggests existing CNS disease
261 knowledge—and even treatment approaches—may be relevant to COVID-19 neuropathology.

262 Genome-wide association studies (GWAS) have shed insight into the molecular
263 pathways involved in complex traits and diseases^{124,125}. GWAS variants suggest an important
264 role for a given gene through its loss or gain of function or expression. Thus, differential
265 expression of GWAS genes in COVID-19 may signal a re-emergence of these trait and disease
266 pathways³². To determine the enrichment of COVID-19 DEGs within genetic variants associated
267 with complex traits and diseases in a cell type-specific fashion, we obtained GWAS summary
268 statistics for neurological and psychiatric disorders and neurobehavior traits (Extended Data
269 Table 8)^{125–127}. We found a strong enrichment of DEGs residing within GWAS hits of various
270 disorders and traits, especially in cognition, schizophrenia, and depression (Fig. 6b). These
271 particular disorders have been associated with dysfunction in L2/3 neurons and astrocytes^{128–}
272 ¹³⁵. Together, these data suggest that COVID-19 may partially recapitulate established
273 pathological processes in the brain and provide molecular hypotheses for emerging neurological
274 complaints in COVID-19 survivors.

275

276 **Discussion**

277 Recent snRNA-seq studies have elucidated the cell type-specific processes involved in
278 several CNS diseases^{32–35,122,123}. Here, by combining sequencing of 47,678 nuclei in both frontal
279 cortex and choroid plexus along with IHC detection of SARS-CoV-2 in brain-barrier cells, we
280 reveal several major neuropathological mechanisms in severe COVID-19. Based on gene
281 expression patterns uncovered in this study, we propose a model where SARS-CoV-2 infected
282 brain-barrier cells can relay and permit inflammatory signaling into the cortex parenchyma. In
283 this inflammatory milieu, peripheral immune cells infiltrate the brain, microglia activate neuronal
284 phagocytosis programs, and astrocyte homeostatic properties become dysregulated. Microglial
285 activation is sufficient to induce a COVID-19 specific subpopulation. Together, these
286 perturbations may converge on impaired neuronal function, with L2/3 excitatory neurons in
287 particular exhibiting a transcriptomic signature of compromised glutamate transmission and
288 information processing^{4,119,120}.

289 There are, however, limitations to consider given the unique logistical circumstances of a
290 pandemic. With most postmortem COVID-19 brain tissue immediately fixed⁴² or not handled
291 with snRNA-seq studies in mind for safety and regulatory reasons, there is a lack of the high-
292 quality tissue necessary for such studies^{21,23,24}. This has precluded larger study cohorts that
293 could be more representative of COVID-19 patients as a whole. For example, while we and a

294 recent IHC-based study of 43 patient brains⁵ (the largest to date) do not find a clear correlation
295 between detectable brain SARS-CoV-2 and glial inflammation or neurological symptoms, this
296 may not be representative of all patients, especially those without pre-existing co-morbidities or
297 who do not require ventilation¹³⁶. Furthermore, the associations with chronic CNS disease may
298 not be relevant in mild COVID-19 disease and may change over time in severe COVID-19
299 survivors. Long-term postmortem studies of survivors after the acute phase of disease are not
300 currently possible to assess this. However, there is precedent for acute viral infections causing
301 long-term inflammation and dysfunction predisposing neurodegenerative disease^{137–140}.

302 Understanding the underlying mechanisms of how SARS-CoV-2 affects the brain may
303 inform therapeutic approaches¹²¹. Most molecular studies to date on SARS-CoV-2 neurotropism
304 have made powerful use of cultured organoids, though they have reached conflicting
305 conclusions^{21–26}. Here, in postmortem COVID-19 patient tissue, we find that the blood-brain and
306 blood-CSF barrier cells typically lacking in organoid models are of high physiologic relevance in
307 informing questions of neurotropism. By combining IHC with a new method to process human
308 choroid plexi tissue for snRNA-seq, we propose that infection of brain-barrier cells can generate
309 a depot of strong antiviral inflammation and compromise barrier function, combining to inflame
310 the brain parenchyma. Such brain-barrier relay and permeability mechanisms have been found
311 important in brain aging^{59,141–144}. Thus, COVID-19's impact on the brain, like many of its other
312 properties, may follow a nuanced—but potentially therapeutically targetable—mechanism of
313 action. We propose that the development of new techniques to study human brain-barrier cells
314 will further help elucidate disease processes in COVID-19 and beyond.

315 The scale of the COVID-19 pandemic means thousands of people may suffer
316 neurological symptoms, with some facing lifelong problems as a result. Our results nominate
317 COVID-19 pathologic processes in microglia, astrocytes, and neurons not seen in a patient
318 suffering terminal influenza infection. The particular vulnerability of layer 2/3 excitatory neurons
319 in COVID-19 provides a consistent molecular hypothesis for emerging neurological complaints,
320 from “brain fog” to memory loss to difficulty concentrating^{11,145,146}. Several COVID-19
321 perturbations revealed here may be addressable with existing medications¹⁴⁷. However, as is
322 the case for recent human transcriptomic studies, additional research will be required to link the
323 observed cell type-specific gene expression changes with neurological symptoms^{32,33,35,122,123}.
324 Nevertheless, these studies have served as important resources for understanding the
325 molecular and cellular basis of disease and for formulating new lines of investigation. In
326 summary, this work sheds insight into and provides new opportunities to explore the acute and
327 lasting neurological consequences of COVID-19.

Acknowledgments

We thank N. Khouri, T. Iram, E. Tapp, O. Hahn, and other members of the Wyss-Coray and Keller labs for feedback and support, and H. Zhang and K. Dickey for laboratory management. This work was funded by the NOMIS Foundation (T.W.-C.), the National Institute on Aging (T32-AG0047126 to A.C.Y., 1RF1AG059694 to T.W.-C), Nan Fung Life Sciences (T.W.-C.), the Bertarelli Brain Rejuvenation Sequencing Cluster (an initiative of the Stanford Wu Tsai Neurosciences Institute), and the Stanford Alzheimer's Disease Research Center (P30 AG066515). A.C.Y was supported by a Siebel Scholarship. F.K., G.S., T.F., W.S.-S., and A.K., are a part of the CORSAAR study supported by the State of Saarland, the Saarland University, and the Rolf M. Schwiete Stiftung.

Author contributions

A.C.Y., F.K., A.K. and T.W.-C. conceptualized the study. M.W.M., N.L., I.C., W.S.-S., N.S., D.C., D.B., and A.C.Y. provided and organized tissue samples. A.C.Y. performed tissue dissociations. A.C.Y., N.S., D.P.L., R.T.V., D.G., and K.C. prepared libraries for sequencing. F.K., G.S., T.F., and A.C.Y. performed computational analysis, with F.K. leading advanced analysis and data management. P.M.L. developed the searchable web interface (Shiny app). W.S.-S. performed immunohistochemical stains. A.C.Y. and C.A.M. assembled figures. A.C.Y. wrote the manuscript with input from all authors. T.W.-C. and A.K. supervised the study.

Competing interests

T.W.-C. is a founder and scientific advisor of Alkahest Inc.

Correspondence and requests for materials should be addressed to A.K. or T.W.-C. (andreas.keller@ccb.uni-saarland.de, twc@stanford.edu).

Figures

Figure 1. Cell type-specific gene expression changes in the brain of COVID-19 patients.

- a**, Study design. Colored triangles denote brain regions studied for each patient.
- b**, Uniform Manifold Approximation and Projection (UMAP) of 23,626 nuclei captured from the human medial frontal cortex, colored by cell type and labeled with percent of total nuclei. Note, that as in prior reports^{32,34,35}, the 'Endothelial' cluster also exhibits vascular mural cell markers.
- c**, Differentially expressed gene (DEG) counts for each cell type (MAST with default thresholds, FDR < 0.05, Log (fold change) > 0.25 (absolute value)). The intensity of the blue color and the size of the squares are proportional to entry values.
- d**, Example differentially expressed genes (DEGs) in COVID-19: excitatory (Ex N) and inhibitory (In N) neurons, astrocytes (Ast), oligodendrocytes (Oli), oligodendrocyte precursor cells (OPC), and microglia (Mic).
- e**, Matrix layout for intersections of DEGs shared across and specific to each cell type. Circles in the matrix indicate sets that are part of the intersection, showing that most DEGs are cell type-specific.
- f**, Fraction of total up- and downregulated genes (y-axis) as a function of the total number of cell types in which the differential expression occurs. Biological pathways associated with genes downregulated in COVID-19 that are common to ≥ 2 cell types are shown ($n = 161$ genes, hypergeometric test, FDR correction).

Figure 1. Cell type-specific gene expression changes in the brain of COVID-19 patients.

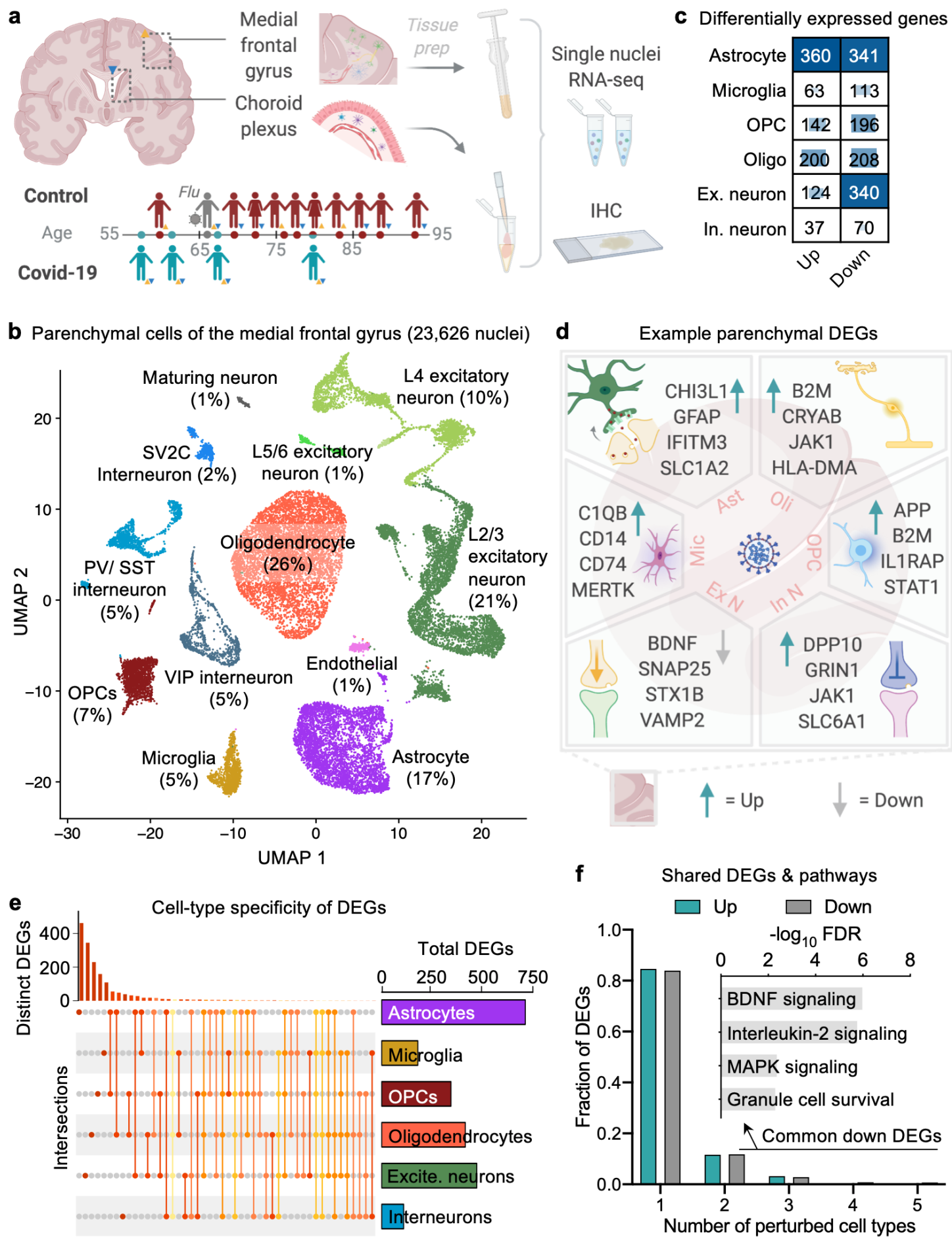


Figure 2. SARS-CoV-2 infection of blood-brain and -CSF barrier cells.

a, SARS-CoV-2 spike glycoprotein (brown) detection in the frontal medial cortex of two COVID-19 patients in tissue immediately adjacent to that used for snRNA-seq. Hematoxylin counterstain (blue). Scale bar = 20 microns.

b, As in **(a)** but for the meninges in Patient 2. Scale bar = 20 microns.

c, As in **(a)** but for the choroid plexi immediately adjacent to tissue used for snRNA-seq, in Patient 1. Scale bar = 20 microns.

Figure 2. SARS-CoV-2 infection of blood-brain and -CSF barrier cells.

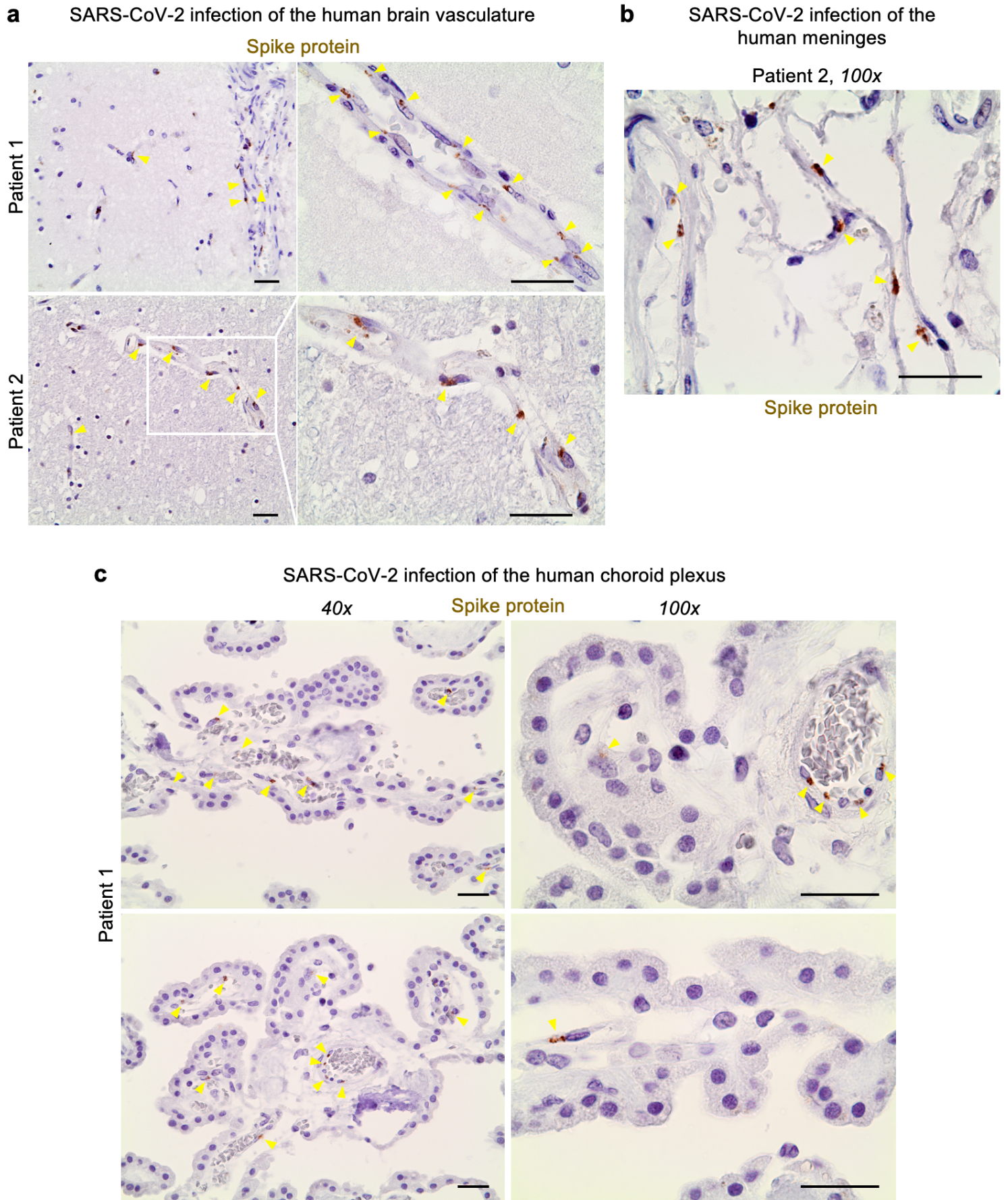


Figure 3. Viral defense and inflammatory signaling in blood-CSF barrier cells.

a, UMAP of 24,052 nuclei captured from the human lateral choroid plexus, colored by cell type and labeled with percent of total nuclei.

b, Expression profiles (CPM, circle size) and differential expression in COVID-19 patients (Log (fold change), color) for genes relevant to SARS-CoV-2 brain entry¹⁶. Grey indicates genes consistently upregulated in either brain-barrier cells (*IFITM3*) or cortex (*NRP1*).

c, DEG counts for each cell type (MAST, FDR < 0.05, Log (fold change) > 0.25 (absolute value)). The intensity of the blue color and the size of the squares are proportional to entry values.

d, Example DEGs in COVID-19 choroid plexus.

e, Matrix layout for intersections of DEGs shared across and specific to each cell type.

f, Circle plot showing the number of statistically significant intercellular signaling interactions for the CCL and CXCL family of molecules in controls (non-viral and influenza) compared to COVID-19 patients (permutation test, CellChat⁶¹).

Figure 3. Viral defense and inflammatory signaling in blood-CSF barrier cells.

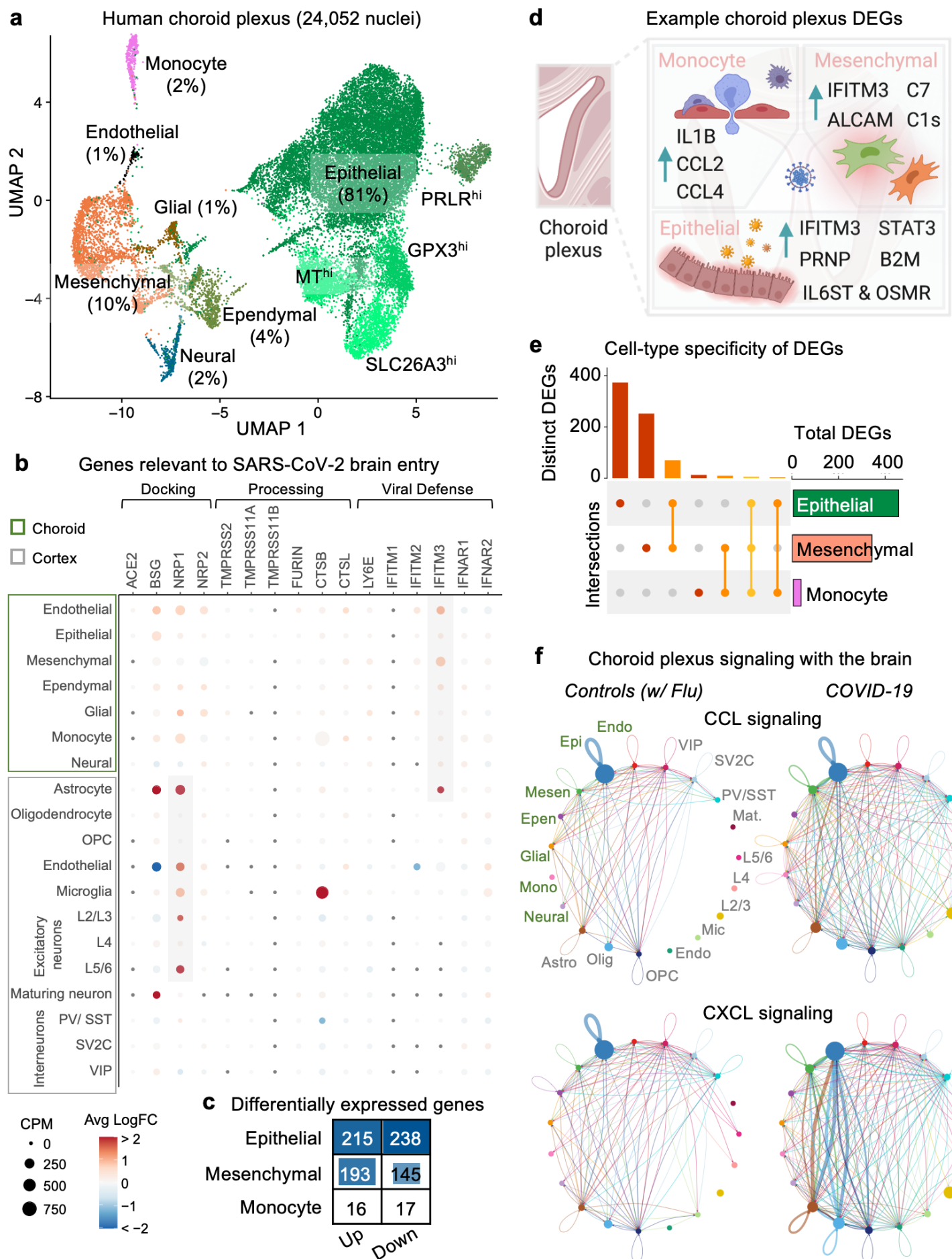


Figure 4. Immune cell infiltration and activation of microglial phagocytosis programs in COVID-19 brains.

a, UMAP of 1,154 immune cells captured in the human frontal cortex, split by non-viral controls, influenza, and COVID-19 patients. Cells are colored by cell type subcluster. Example genes upregulated in Microglia cluster 2 are shown.

b, Quantification of Microglia 2 population as a proportion of total immune cells ($n = 5$ controls, including influenza; $n = 4$ COVID-19, two-sided t-test; mean +/- s.e.m.).

c, Monocle⁶⁴ pseudotime trajectory plotting the emergence of Microglia cluster 2. Pseudotime is indicated in graded purple (high) to yellow (high). Numbers indicate Microglial cluster from **(a)**.

d, Quantification of the T-cell population as a proportion of total immune cells ($n = 5$ controls, including influenza; $n = 4$ COVID-19, two-sided t-test; mean +/- s.e.m.).

e, Expression of the established peripheral macrophage-specific marker *F13A1*^{65,66}. Expression (logCPM) is indicated in graded purple (left). Quantification of the peripheral macrophage population as a proportion of total immune cells ($n = 5$ controls, including influenza; $n = 4$ COVID-19, two-sided t-test; mean +/- s.e.m., right).

f, Expression of established microglial activation^{67–74} and inflammation checkpoint^{75–77} molecules. Violin plots are centered around the median, with their shape representing cell distribution (** $P < 0.001$, **** $P < 0.00001$, MAST).

g, Upregulation of genes mediating the microglial phagocytosis of live neurons⁸¹. Bold indicates upregulated genes in COVID-19, grey not detected.

Figure 4. Immune cell infiltration and activation of microglial phagocytosis programs in COVID-19 brains.

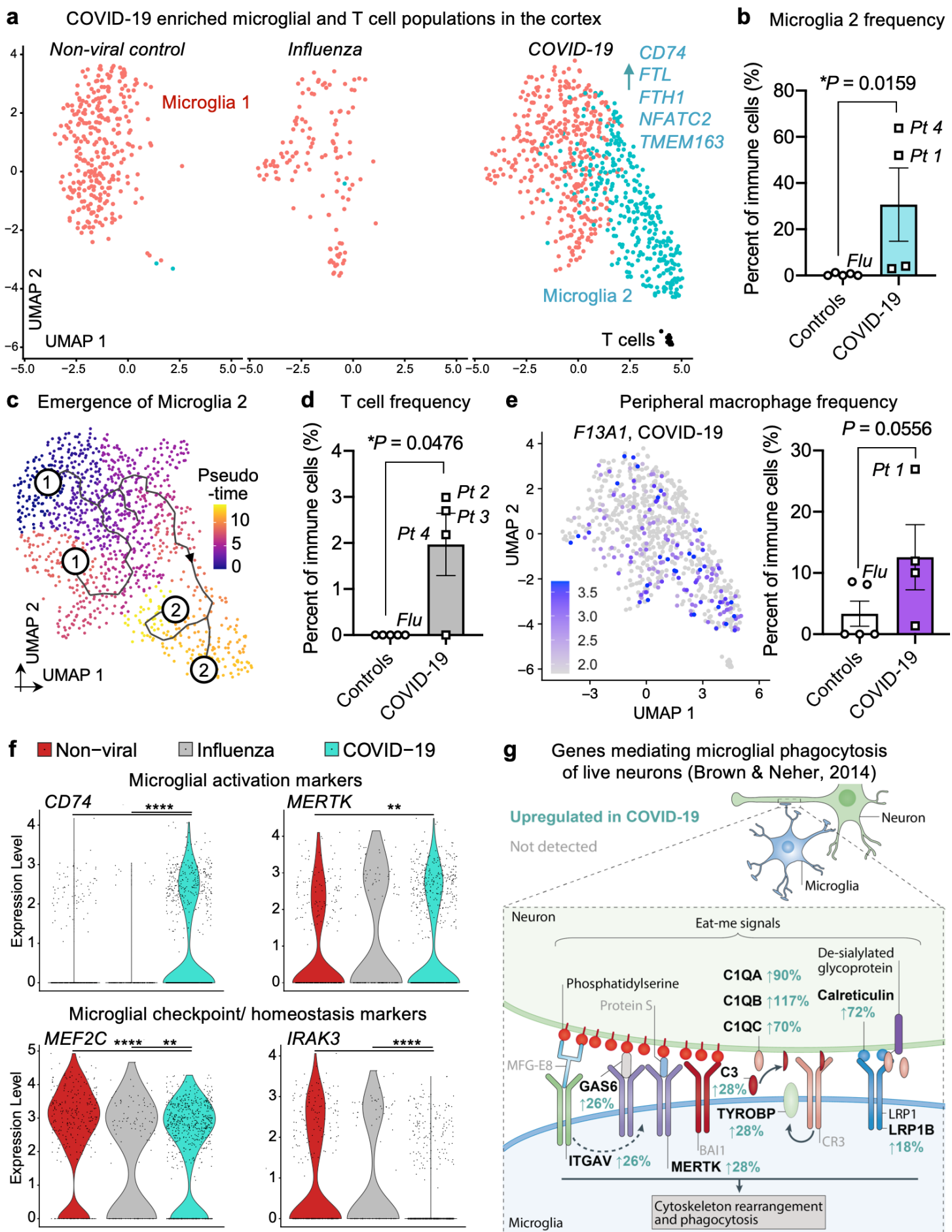


Figure 5. Impaired astrocytic support and excitatory neurotransmission in COVID-19 cortex.

- a**, Upregulation of inflammatory and dysregulation of homeostatic genes in COVID-19 astrocytes ($n = 3,967$).
- b**, Enriched biological pathways (Elsevier Pathway Collection, Enrichr) amongst upregulated genes in COVID-19 astrocytes. Enrichment is based on FDR-corrected cumulative hypergeometric P values, with a P value-thresholded DEG gene-marker list ($\log(\text{fold change}) > 0.25$ (absolute value), adjusted P value (Bonferroni correction) < 0.05 , MAST).
- c**, UMAP of 3,967 astrocytes captured in the human frontal cortex, split by non-viral controls, influenza, and COVID-19 patients. Cells are colored by cell type subcluster. Example genes upregulated in Astrocyte cluster 3 are shown.
- d**, Quantification of Astrocyte 3 population as a proportion of all astrocytes ($n = 5$ controls, including influenza; $n = 4$ COVID-19, two-sided t-test excluding influenza patient; mean +/- s.e.m.).
- e**, Expression of homeostatic astrocyte glutamate transporter genes encoding EEAT2 (*SLC1A2*) and EEAT1 (*SLC1A3*). Violin plots are centered around the median, with their shape representing cell distribution (** $P < 0.0001$, MAST).
- f**, Downregulation of major SNARE components in COVID-19 excitatory neurons ($n = 7,680$ excitatory neurons).
- g**, Heatmap showing downregulation of synaptic vesicle components specifically in COVID-19 L2/3 excitatory neurons ($n = 7,680$ excitatory neurons; $n = 4,948$ L2/3 excitatory neurons, $\log(\text{fold change}) > 0.25$ (absolute value), adjusted P value (Bonferroni correction) < 0.05 , MAST).

Figure 5. Impaired astrocytic support and excitatory neurotransmission in COVID-19 cortex.

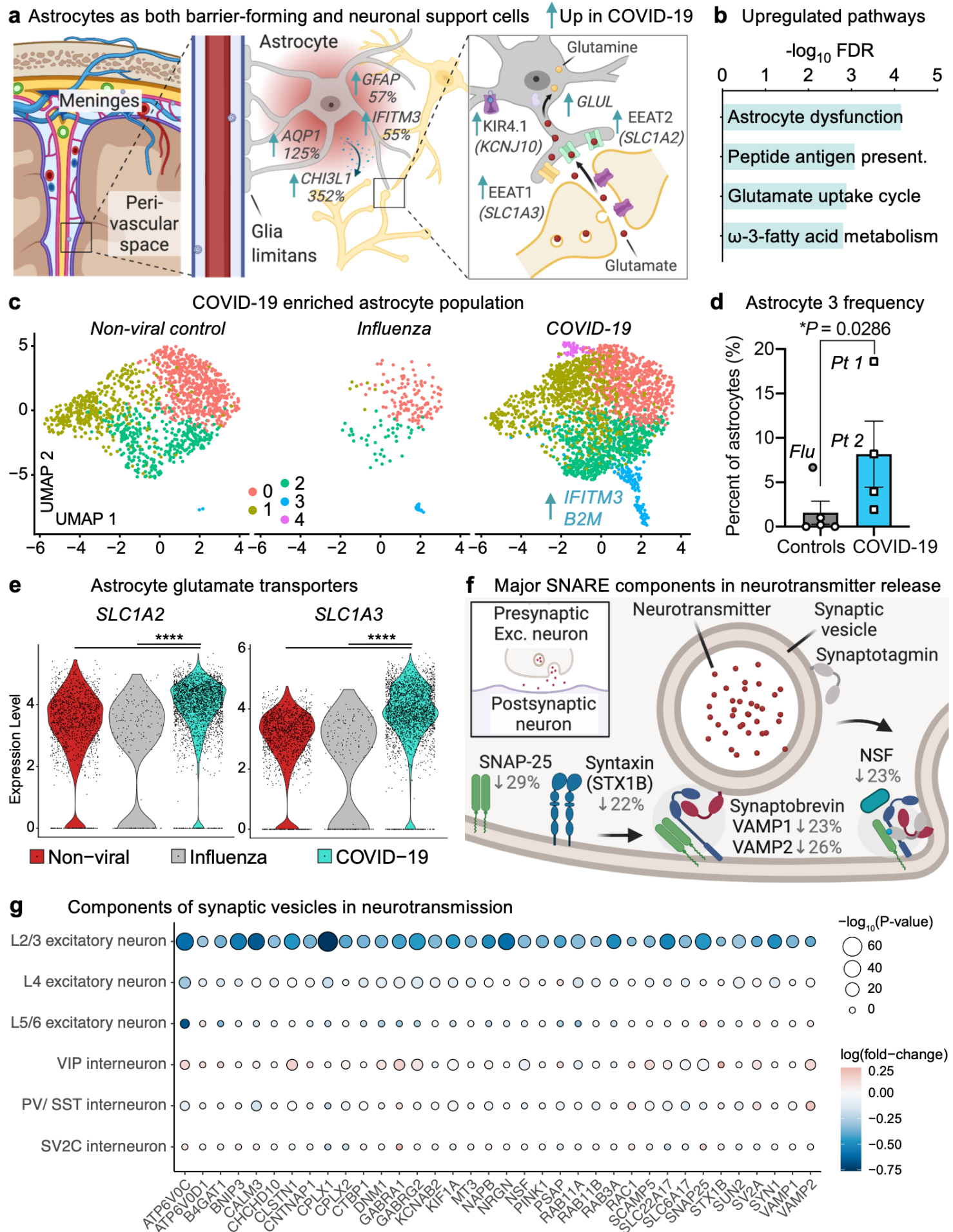


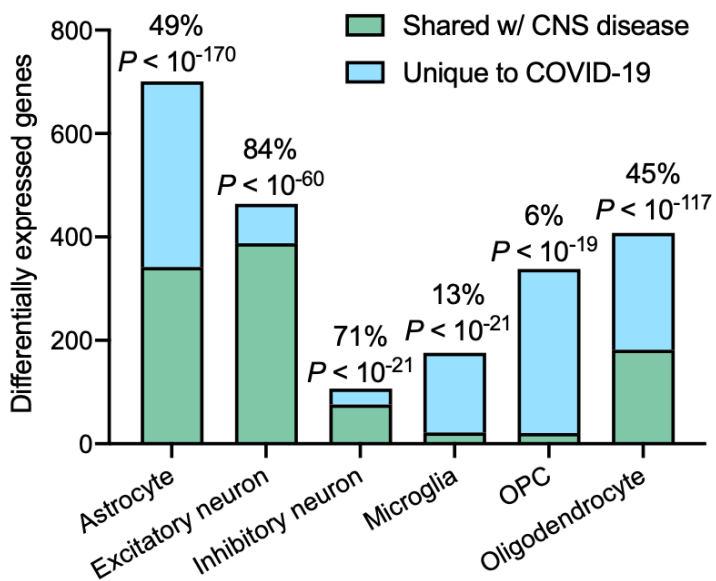
Figure 6. Association of COVID-19 gene expression changes with chronic CNS disease.

a, Proportion of COVID-19 DEGs across cell types that are also DEGs in chronic CNS diseases, as published for Alzheimer's Disease (AD)³⁴, Autism spectrum disorder (ASD)³³, Huntington's disease (HD)¹²³, and Multiple sclerosis (MS)¹²². Bars labeled with percent overlapping and over-representation *P* values (cumulative hypergeometric test).

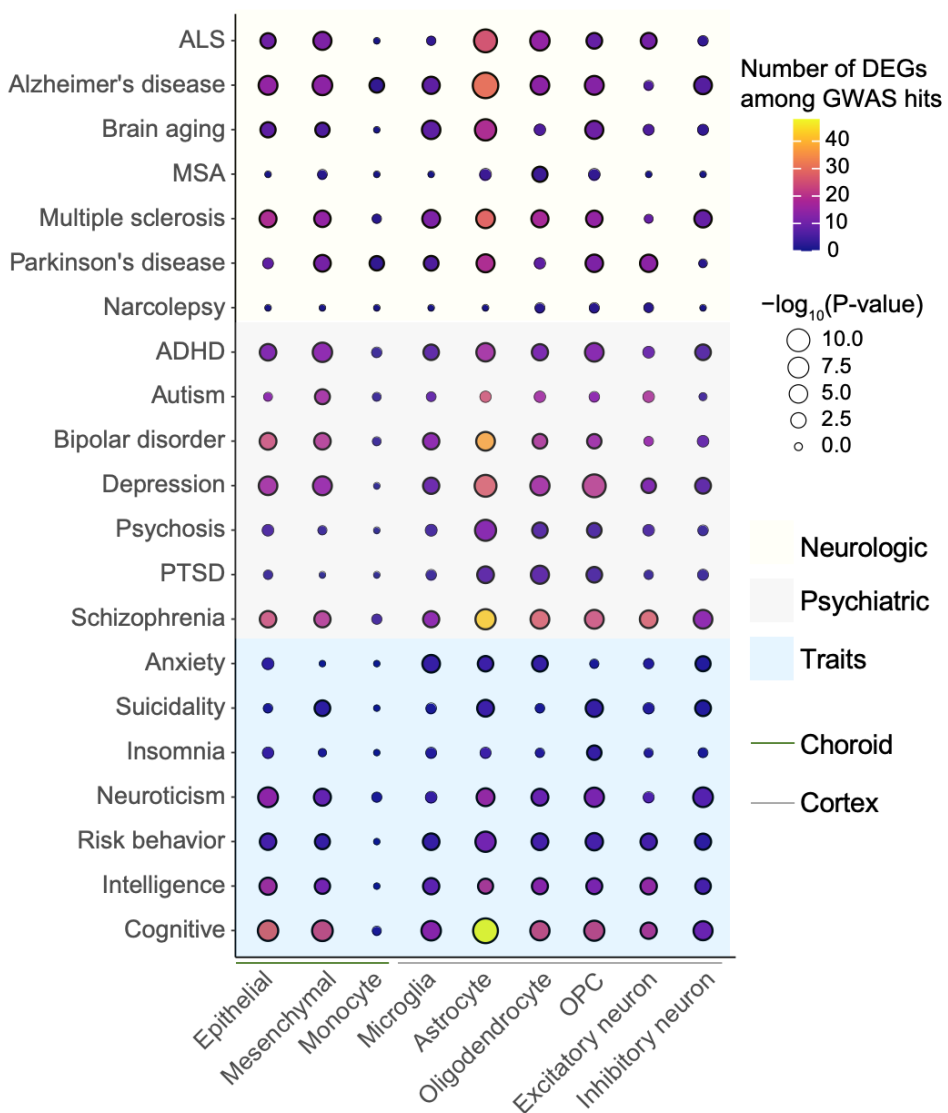
b, Heatmap showing the number of differentially expressed genes (DEGs) per cell type that are also GWAS risk variants across psychiatric and neurological diseases and traits from the GWAS catalog (NHGRI-EBI)¹²⁶. Significance is based on FDR-corrected cumulative hypergeometric *P* values, with a *P* value-thresholded DEG list ($\log(\text{fold change}) > 0.25$ (absolute value), adjusted *P* value (Bonferroni correction) < 0.05 , MAST). ALS: Amyotrophic lateral sclerosis, MSA: Multiple system atrophy, ADHD: Attention deficit hyperactivity disorder, and PTSD: Post-traumatic stress disorder.

Figure 6. Association of COVID-19 gene expression changes with chronic CNS disease.

a Comparison of COVID-19 DEGs w/ CNS diseases



b Cell type-specific transcriptomic changes in CNS disease GWAS genes



Methods

Isolation of nuclei from frozen post-mortem medial frontal gyrus

Frozen medial frontal cortex tissue from post-mortem control and COVID-19 patients were obtained from the Stanford/ VA/ NIA Aging Clinical Research Center (ACRC) and the Saarland University Hospital Institute for Neuropathology, with approval from local ethics committees. Group characteristics are presented in Supplementary Table 1. The protocol for the isolation of nuclei was adapted from previous studies^{32,34,35,148,149}, and performed in a BSL2+ Biosafety Cabinet wearing PPE. All procedures were carried out on ice or at 4°C. Briefly, 50 mg of post-mortem brain tissue was dounce homogenized in 2 ml of Nuclei EZ Prep Lysis Buffer (Sigma, NUC101) spiked with 0.2 U μl^{-1} RNase inhibitor (Takara, 2313A) and EDTA-free Protease Inhibitor Cocktail (Roche, 11873580001) before incubating on ice for 5 min in a final volume of 5 ml. Homogenized tissue was filtered through a 100- μm cell strainer (Falcon, 352360), mixed with an equal volume of 50% iodixanol density gradient medium in PBS (OptiPrep, Sigma-Aldrich, D1556) to make a final concentration of 25% iodixanol. 30% iodixanol was layered underneath the 25% mixture. Similarly, 40% iodixanol was layered underneath the 30% iodixanol. In a swinging-bucket centrifuge, nuclei were centrifuged for 20 min at 3,000 r.c.f. After centrifugation, the nuclei were present at the interface of the 30% and 40% iodixanol solutions. Isolated nuclei were resuspended in 1% BSA with 0.2 U μl^{-1} RNase inhibitor, filtered twice through a 40 μm strainer (Flowmi), and counted on an TC20 automated cell counter (Bio-Rad) after the addition of Trypan Blue. We did not use statistical methods to pre-determine sample sizes, but our sample sizes are similar to those reported in previous publications^{30–32}.

Isolation of nuclei from frozen post-mortem choroid plexus

Frozen choroid plexus tissue was extracted from the lateral ventricles of post-mortem tissue obtained from the Stanford University Pathology department and the Saarland University Hospital Institute for Neuropathology, with approval from local ethics committees. Group characteristics are presented in Supplementary Table 1. All procedures were carried out on ice or at 4°C, and in a BSL2+ Biosafety Cabinet wearing PPE. Dounce homogenization or enzymatic dissociation successfully used for mice choroid plexi²⁹ resulted in loss of nuclei integrity and low nuclei complexity (<50 median genes/ nuclei). We hypothesized that like shaking an apple tree, gentle pipetting of choroid plexus tissue in lysis buffer could liberate nuclei without needing to physically disintegrate the fibrous choroid matrix—and thus avoid collateral physical damage to nuclei. Specifically, 40 mg of choroid plexus tissue was thawed in 250 μl of 1% BSA with 0.2 U μl^{-1} RNase inhibitor until the tissue settled. 5 ml of lysis buffer (10 mM Tris, 10 mM NaCl, 3 mM MgCl₂, 0.1% Nonidet P40 substitute (Roche/ Sigma, 11754599001), 0.2 U μl^{-1} RNase inhibitor, and protease inhibitor) was added and tissue incubated on ice for 10 minutes with gentle swirling every 2 minutes. 5 ml of 1% BSA was added and the tissue triturated 10 times with a 5 ml serological pipette. After centrifugation (500g, 5 min), pelleted nuclei were resuspended in 1% BSA with 0.2 U μl^{-1} RNase inhibitor; gently triturated 10 times with a 1 ml regular-bore pipette tip; and filtered twice through a 70 μm and then a 40 μm strainer (Flowmi). Debris was inspected on a brightfield microscope and nuclei were counted on an TC20 automated cell counter (Bio-Rad) after the addition of Trypan Blue.

Droplet-based snRNA-sequencing

For droplet-based snRNA-seq, libraries were prepared using the Chromium Next GEM Single Cell 3' v3.1 according to the manufacturer's protocol (10x Genomics), targeting 10,000 nuclei per sample after counting with a TC20 Automated Cell Counter (Bio-Rad). 13 cycles were applied to brain parenchyma samples to generate cDNA, and 15 for choroid plexus samples. All samples underwent 15-16 cycles for final library generation. Generated snRNA-seq libraries were sequenced across two S4 lanes on a NovaSeq 6000 (150 cycles, Novogene).

snRNA-seq quality control

Gene counts were obtained by aligning reads to the hg38 genome (refdata-gex-GRCh38-2020-A) using CellRanger software (v.4.0.0) (10x Genomics). To account for unspliced nuclear transcripts, reads mapping to pre-mRNA were counted. As previously published, a cut-off value of 200 unique molecular identifiers (UMIs) was used to select single nuclei for further analysis³⁴. As initial reference, the entire dataset was projected onto two-dimensional space using Uniform Manifold Approximation and Projection (tSNE) on the top 20 principal components¹⁵⁰. Three approaches were combined for quality control: (1) ambient cell free mRNA contamination was removed using SoupX¹⁵¹ for each individual sample; (2) outliers with a high ratio of mitochondrial (>5%, <200 features) relative to endogenous RNAs and homotypic doublets (> 5000 features) were removed in Seurat¹⁵²; and (3) after scTransform normalization and integration, doublets and multiplets were filtered out using DoubletFinder with subsequent manual inspection and filtering based on cell type-specific marker genes¹⁵³. Genes detected in fewer than 4 cells were excluded. After applying these filtering steps, the dataset contained 47,678 high-quality nuclei.

Cell annotations

Seurat's Integration function was used to align data with default settings. Genes were projected into principal component (PC) space using the principal component analysis (RunPCA). The first 80 (for global object), 30 (choroid plexus), or 25 (specific cell types) dimensions were used as inputs into Seurat's FindNeighbors, FindClusters (at 0.2 resolution) and RunUMAP functions. Briefly, a shared-nearest-neighbor graph was constructed based on the Euclidean distance metric in PC space, and cells were clustered using the Louvain method. RunUMAP functions with default settings was used to calculate 2-dimensional UMAP coordinates and search for distinct cell populations. Positive differential expression of each cluster against all other clusters (MAST) was used to identify marker genes for each cluster¹⁵⁴. We annotated cell-types using previously published marker genes^{31,33–35}.

Differential gene expression and sub-cluster analysis

Differential gene expression of genes comparing controls, COVID-19, and influenza samples—or comparing cell type sub-cluster markers—was done using the MAST¹⁵⁴ algorithm, which implements a two-part hurdle model. Seurat default Log (fold change) > 0.25 (absolute value), adjusted P value (Bonferroni correction) < 0.05, and expression in greater than 10% of cells were required to consider a gene differentially expressed. Biological pathway and gene ontology enrichment analysis was performed using Enrichr¹⁵⁵, Metascape¹⁵⁶, or GeneTrail 3¹⁵⁷ with input species set to *Homo sapiens*¹⁵⁶ and using standard parameters. Docking, processing, and viral defense genes relevant to SARS-CoV-2 were chosen based on Iadecola, et al¹⁶. To identify microglia sub-cluster markers, differential expression analysis of cells grouped in each sub-cluster was performed against the remaining cells within the given cell-type. Markers were defined based on the MAST algorithm using only positive values with Log (fold change) > 0.25 (absolute value), adjusted P value (Bonferroni correction) < 0.01. Enrichment/ over-representation of the overlap between markers defining the COVID-19 microglia 2 cluster and the Mathys³⁴ Alzheimer's disease Mic1 cluster followed the hypergeometric probability, using the set of 17,926 protein-coding genes as background.

Monocle trajectory analysis

Monocle3 (v.0.2.1.) was used to generate the pseudotime trajectory analysis in microglia⁶⁴. Cells were re-clustered as above and used as input into Monocle to infer cluster and lineage relationships within a given cell type. Specifically, tSNE embeddings and cell sub-clusters generated from Seurat were converted to a *cell_data_set* object using SeuratWrappers (v.0.2.0)

and then used as input to perform trajectory graph learning and pseudo-time measurement through reversed graph embedding with Monocle.

Viral transcripts

To search for SARS-CoV-2 reads, raw fastq files were subjected to read alignment via Viral-Track¹⁵⁸ or centrifuge¹⁵⁹ using the human (GRCh38) genome reference. For Viral-Track both a collection of 12,163 consensus virus sequences from Virusite¹⁶⁰ (release 2020.3) and 17,133 curated SARS-CoV-2 genomes from NCBI (downloaded on 29-09-2020) were used. For centrifuge, a preprocessed virus index compiled by genexa containing among other viruses 138 SARS-CoV-2 genomes was used. We also adopted a complementary approach¹⁶¹ focusing on SARS-CoV-2 reads, whereby barcoded but unmapped BAM reads were aligned using STAR to the SARS-CoV-2 reference genome, with a less stringent mapping parameter (outFilterMatchNmin 25-30) than the original Viral-Track pipeline.

Cell-cell communication

Cell-cell interactions based on the expression of known ligand-receptor pairs in different cell types were inferred using CellChatDB⁶¹ (v.0.02). To identify potential cell-cell communication networks perturbed or induced in COVID-19 patient brains, we focused on differentially expressed ligands in choroid plexus epithelium, microglia, and astrocytes; and differentially expressed receptor pairs in excitatory and inhibitory neurons. Briefly, we followed the official workflow and loaded the normalized counts into CellChat and applied the preprocessing functions *identifyOverExpressedGenes*, *identifyOverExpressedInteractions*, and *projectData* with standard parameters set. As database we selected the *Secreted Signaling* pathways and used the pre-compiled human Protein-Protein-Interactions as a priori network information. For the main analyses the core functions *computeCommunProb*, *computeCommunProbPathway*, and *aggregateNet* were applied using standard parameters and fixed randomization seeds. Finally, to determine the senders and receivers in the network the function *netAnalysis_signalingRole* was applied on the *netP* data slot.

GWAS

From the GWAS catalog¹²⁶, we obtained GWAS risk genes for neurological disorders [Alzheimer's disease (AD), amyotrophic lateral sclerosis (ALS), brain aging, multiple system atrophy (MSA), multiple sclerosis (MS), Parkinson's disease (PD), and narcolepsy], psychiatric disorders [Attention deficit hyperactivity disorder (ADHD), autism, bipolar disorder, depression, psychosis, post-traumatic stress disorder (PTSD), and schizophrenia], and neurobehavior traits [Anxiety, suicidality, insomnia, neuroticism, risk behavior, intelligence, and cognitive function]. We removed gene duplicates and GWAS loci either not reported or in intergenic regions and used a $P < 9 \times 10^{-6}$ to identify significant associations³². Then, since GWAS signals can point to multiple candidate genes within the same locus, we focused on the 'Reported Gene(s)' (genes reported as associated by the authors of each GWAS study). Disorders and traits exhibiting a significant number of genes also perturbed in COVID-19 patients are highlighted. Following gene symbol extraction, we curated the gene set by (1) removing unknown or outdated gene names using the HGNHelper package (v.0.8.6), (2) converting remaining Ensembl gene IDs to actual gene names using the packages ensemblDb (v.2.10.0) and EnsDb.Hsapiens.v86 (v.2.99.0), and (3) removing any remaining duplicates. We then calculated the overlap between each set of GWAS genes with the cell type-specific DEGs. Finally, a statistical enrichment of each overlap against background was calculated using a hypergeometric test with the total background size set equal to the number of unique RNAs mapped in our data set (29,431).

Comparison of DEGs in chronic CNS disease

We compiled cell type-specific differentially expressed genes (DEGs) reported in published datasets for Alzheimer's Disease (AD)³⁴, Autism spectrum disorder (ASD)³³, Huntington's disease (HD)¹²³, and Multiple sclerosis (MS)¹²². Lists of gene symbols were curated using the aforementioned approach. COVID-19 DEGs that overlap with those found across the selected CNS diseases were called shared, whereas those not previously reported were called unique to COVID-19. Statistical significance calculations of over-representation in DEG overlaps are based on cumulative hypergeometric *P* values analogous to the procedure described above.

PVCA and PCA analysis

Briefly, to conduct the Principal Variance Component Analysis (PVCA), we aggregated the *SoupX* corrected raw counts for each gene and each biological sample using the *aggregateData* function of the *muscat* package (v.1.2.1). The resulting matrix was normalized by dividing each feature of a sample by the total counts from that sample, multiplied by a scaling factor of 100,000 and scaling the result using the function $\log(x+1)$. As variables we considered the sample annotation fields "Sample-ID", "Patient-ID", "Sex", "Brain-region", "Disease", "ageBin", and "nNucleiBin". Since the number of nuclei and age are numeric variables but PVCA is designed to support factors, we assigned the values into ordered bins, more specifically, into five half-open (left-closed) intervals of size 1,000 starting at 2,000 for the number of nuclei and five similarly defined intervals of size 10 starting at 51 for the age. We set the algorithm cut-off for the minimal variance out of the total variance being explained to be 95%. For each single annotation variable, or first higher-order combinations of such, at cut-off of 0.005 was applied to consider them explanatory. All variables (or combinations of such) not passing the threshold were summarized as *Other* in the analysis. The residual is then defined as the remaining proportion of variance not being associated with any of the variables that are explanatory nor informative to a minor proportion. To conduct Principal Components Analysis (PCA) we aggregated the log-normalized cell counts from *Seurat* for each gene and sample using the *aggregateData* function from *muscat* and centered the gene expression vectors before computing eigenvectors.

Overall in-silico analysis

Analysis and dissection of the data was performed using the statistical programming language R (v.3.6.3) using the following general-purpose package for loading, saving, and manipulating data, as well as generating plots, and fitting statistical models: *dplyr* (v.1.0.0), *ggplot2* (v.3.2.2.), *patchwork* (v.1.0.1), *openxlsx* (v.4.1.5), *bioconductor-scater* (v.1.14.6), *bioconductor-dropletutils* (v1.6.1), *bioconductor-complexheatmap* (v.2.2.0), *tidyverse* (v.1.3.0), and *lisa* (v.0.73.2). All other tasks were performed on an x86_64-based Ubuntu (4.15.0-55-generic kernel) server cluster.

Immunohistochemistry

Paraffin-embedded human brain tissue (medial frontal cortex, meninges, and choroid plexus) adjacent to tissue processed for snRNA-seq was subjected to immunohistochemistry (IHC). After deparaffinization and rehydration of 1-3 μ m sections, peroxidases were blocked by incubation in 1% H₂O₂ for 15 minutes at room temperature. Heat antigen retrieval was performed by steaming at 98°C in target retrieval solution pH 6.1 (Dako, Carpinteria, CA, USA #S1699) for 30 minutes. Sections were allowed to cool down at room temperature. Following antigen retrieval, sections were incubated for 45 minutes at room temperature with the anti-SARS spike glycoprotein antibody 3A2 (rabbit, Abcam ab272420 1:100 diluted in Dako REAL antibody diluent #S2022), which has been validated in previous publications^{20,41}. After three washes with wash buffer (Dako #S3006), the Dako REAL EnVision HRP kit (#K5007) was used for the visualization of the antibody reaction according to the manufacturer's instructions. Sections were counterstained with Mayer's hemalum (Sigma-Aldrich #1.09249). After

dehydration, coverslips were mounted with Entellan (Merck #1.07961). Images were acquired with an Olympus BX 40 microscope, equipped with an Olympus SC30 digital microscope camera using the Olympus cellSens software.

Data Availability. Raw sequencing data is deposited under NCBI GEO: GSE159812.

Normalized counts data also available for download at:

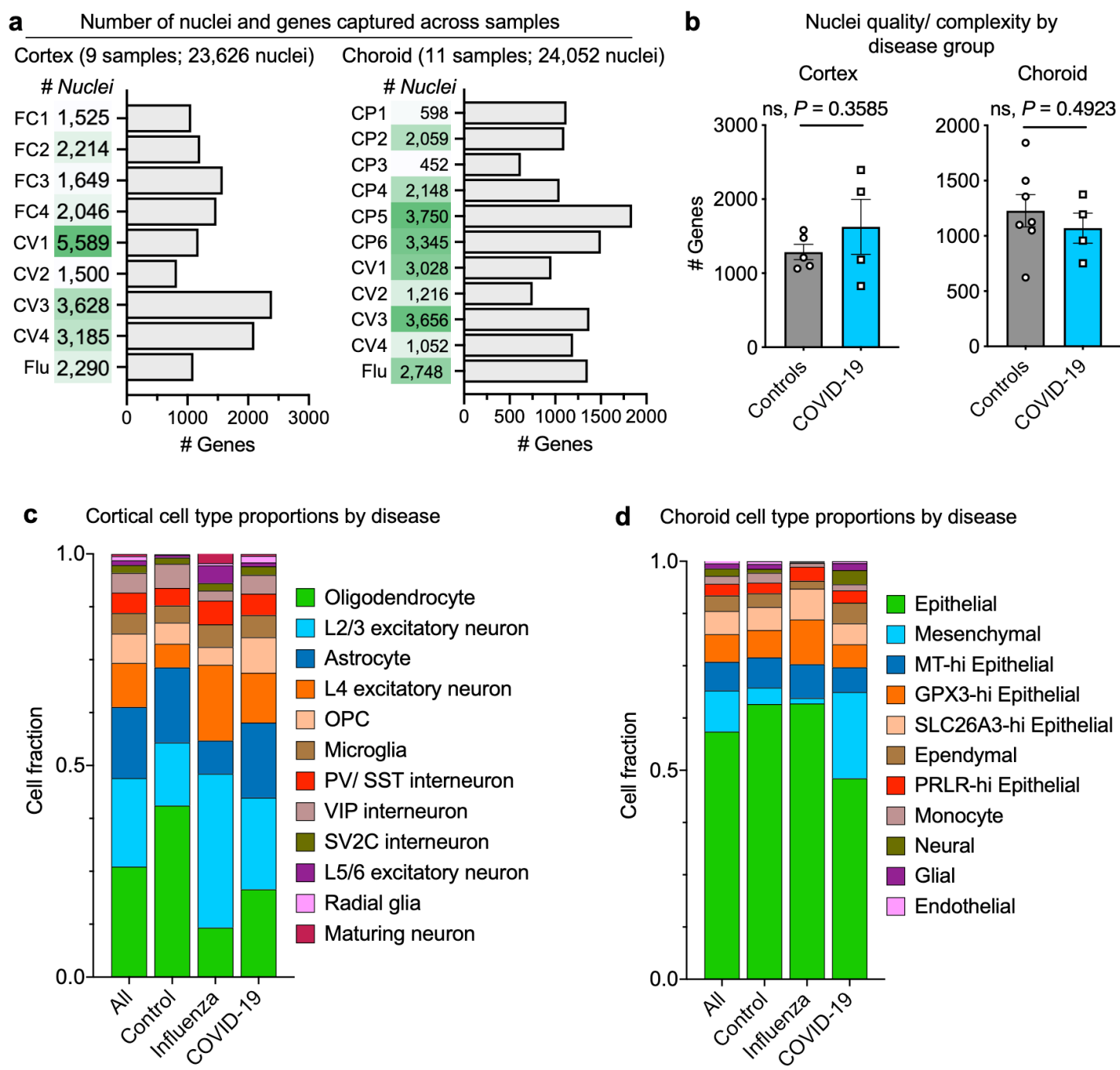
https://tvc-stanford.shinyapps.io/scRNA_Brain_COVID19.

Extended Data Figures

Extended Data Figure 1. Characterization of human cortical and choroid plexi nuclei sequenced.

- a**, Total number of nuclei and median number of genes of each human sample sequenced in medial frontal cortex and choroid plexus.
- b**, Quantification of the median number of genes detected per nuclei in controls (non-viral and influenza) and COVID-19 samples in medial frontal cortex and choroid plexus ($n=5-7$ controls and $n=4$ COVID-19, two-sided t-test; mean +/- s.e.m.).
- c, d**, Bar graph presenting frequency of nuclei for non-viral controls, influenza, and COVID-19 medial frontal cortex (**c**) and choroid plexus (**d**) sample groups.

Extended Data Figure 1. Characterization of human cortical and choroid plexi nuclei sequenced. available under aCC-BY-NC 4.0 International license.

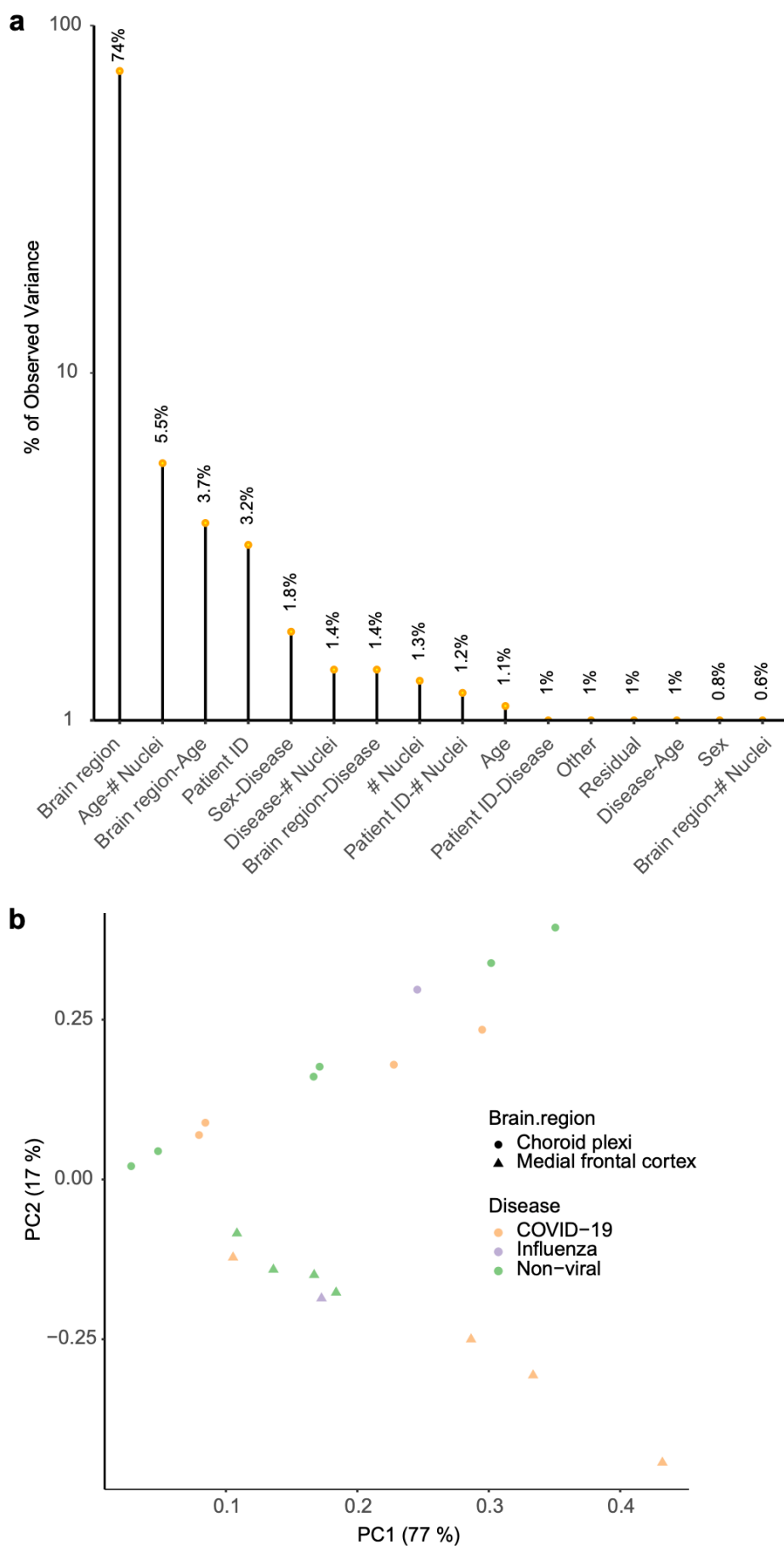


Extended Data Figure 2. Gene expression variance analysis.

a, Principal variance component analysis, displaying the gene expression variance explained by residuals (biological and technical noise) or experimental factors such as brain region, age, sex, and respective combinations. $n = 15$ samples.

b, Principal component analysis (PCA) visualization of all samples, based on unscaled counts.

Extended Data Figure 2. Gene expression variance analysis.



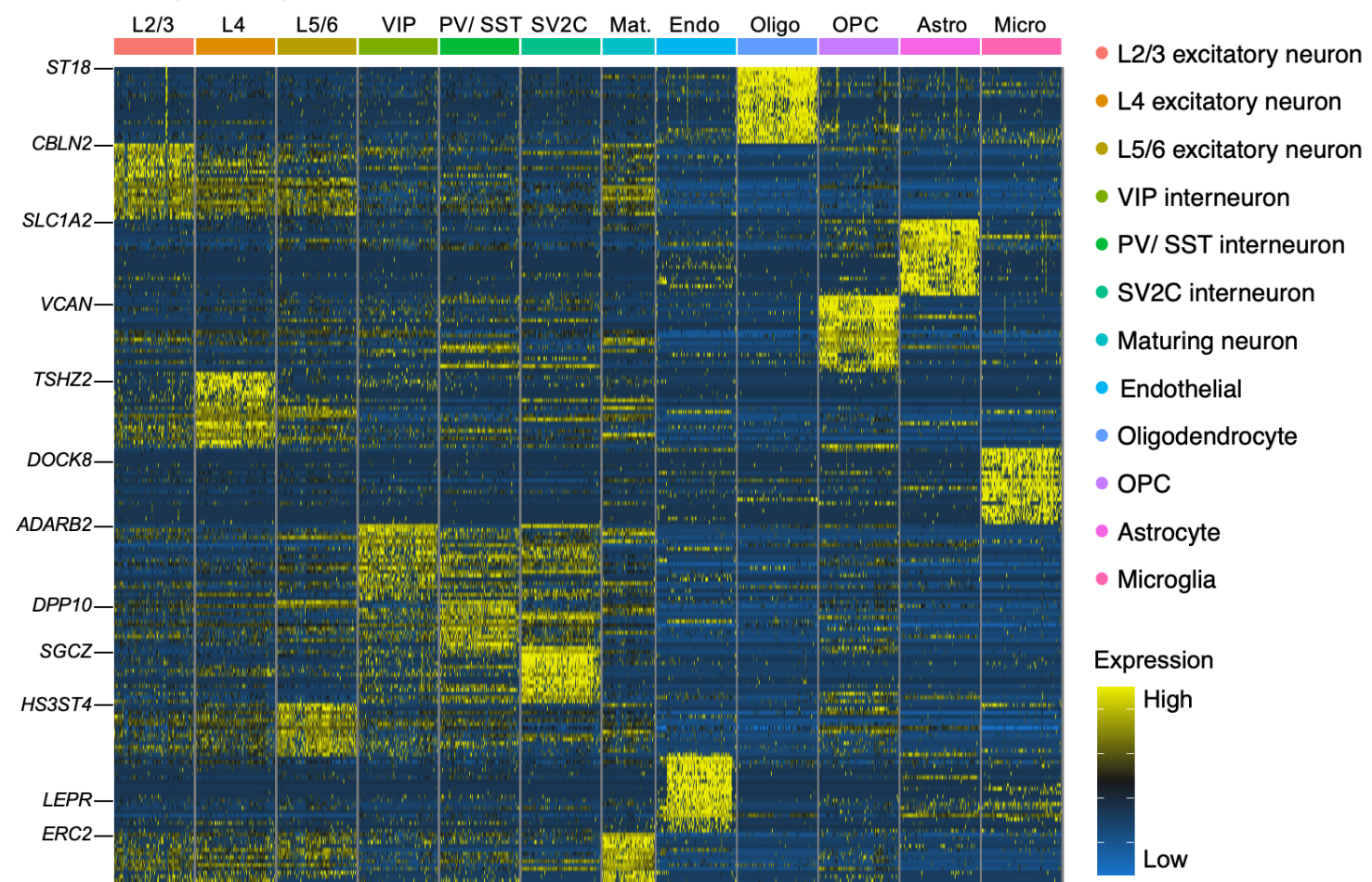
Extended Data Figure 3. Markers for annotating parenchymal cells in the human frontal medial cortex.

a, Discovery of the top cell type-specific genes across the 12 classes of cells captured in the human cortex. The color bar indicates gene expression from low (blue) to high (yellow).

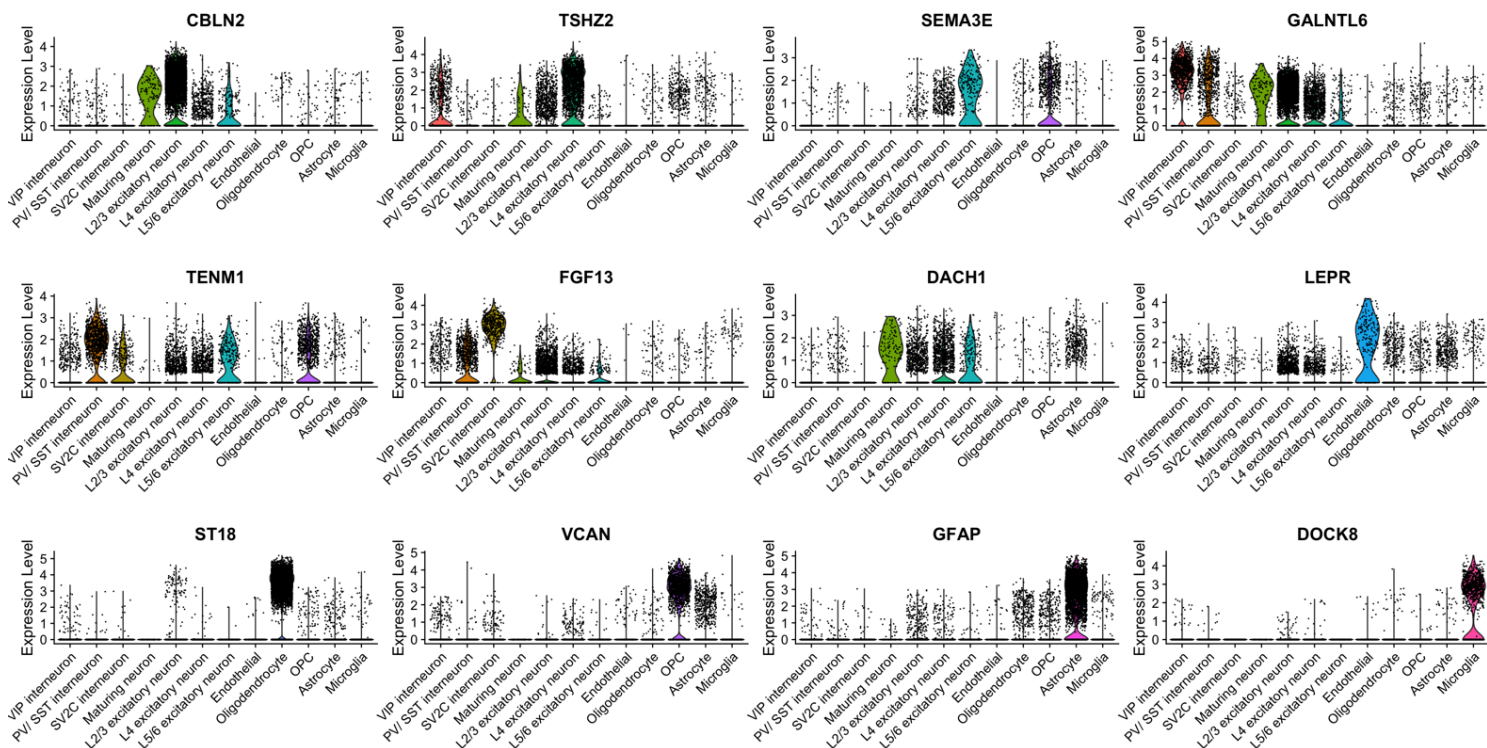
b, Validation of cell type annotations using established cell type-specific markers. Violin plots are centered around the median, with their shape representing cell distribution.

Extended Data Figure 3. Markers for annotating parenchymal cells in the human frontal medial cortex.

a Discovery of cell type-specific markers



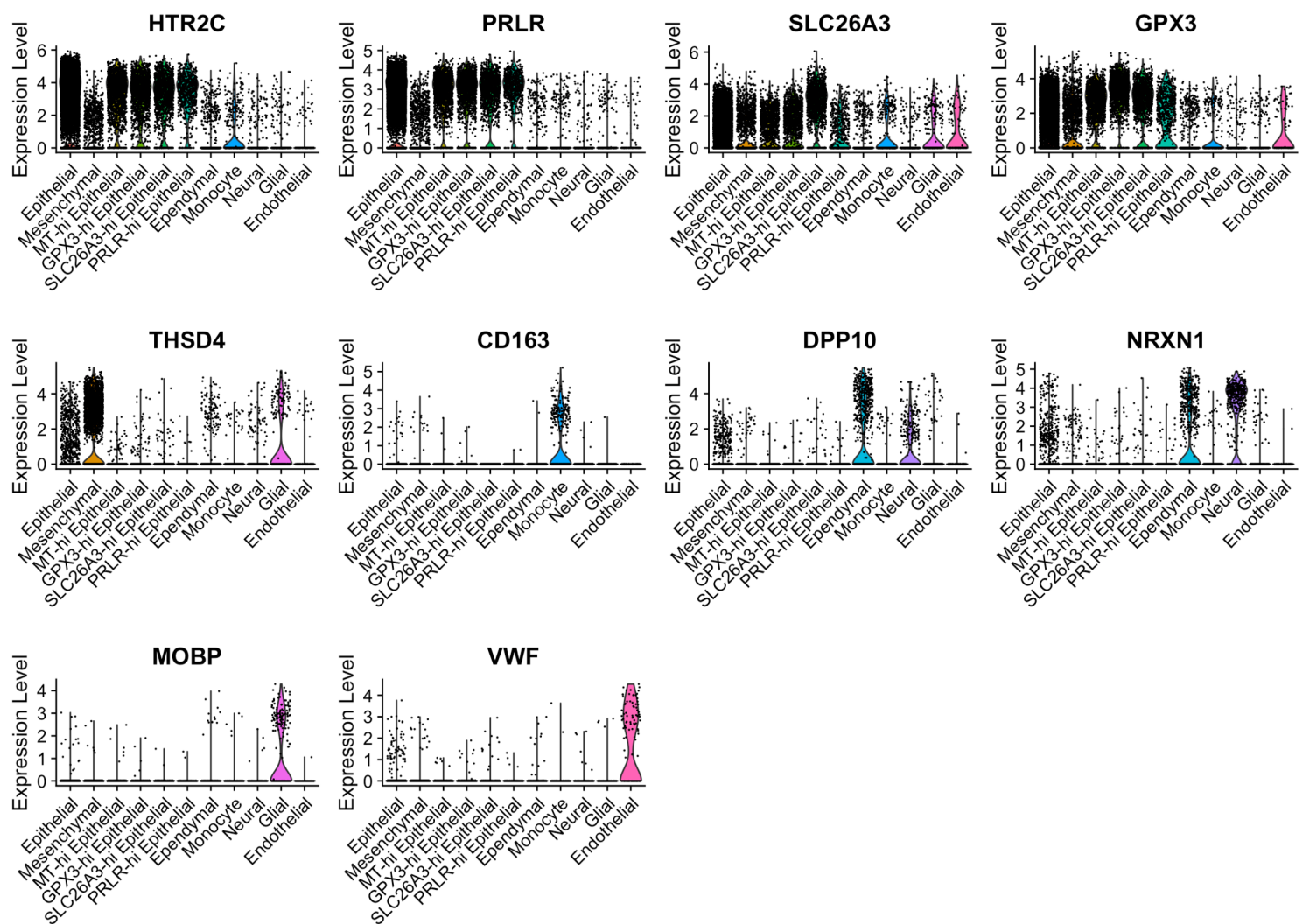
b Validation of cell type annotations



Extended Data Figure 4. Markers for annotating parenchymal cells in the human choroid plexus.

Validation of cell type annotations using established cell type-specific markers. Subsets of epithelial cells are marked by high expression of specific markers not previously described in mice. Violin plots are centered around the median, with their shape representing cell distribution.

Extended Data Figure 4. Markers for annotating parenchymal cells in the human choroid plexus.



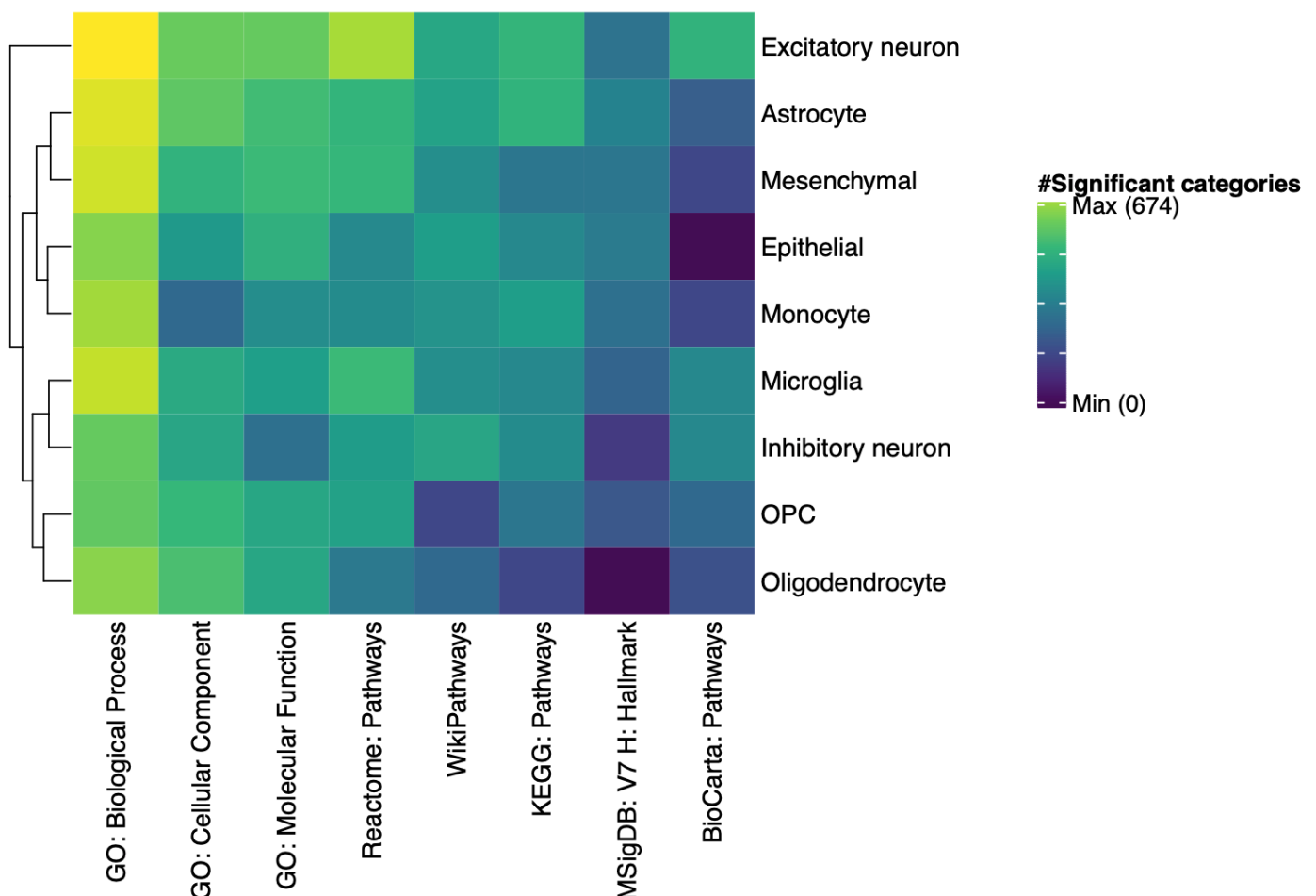
Extended Data Figure 5. Cell-type specific changes in gene expression and intercellular signaling in the COVID-19 brain.

a, Heatmap displaying the number of significant biological pathways among the set of differentially expressed genes in each cell type (FDR < 0.05, Fisher's exact test with Benjamini-Hochberg correction). Number of significant pathways is indicated in graded black (high) to yellow (high).

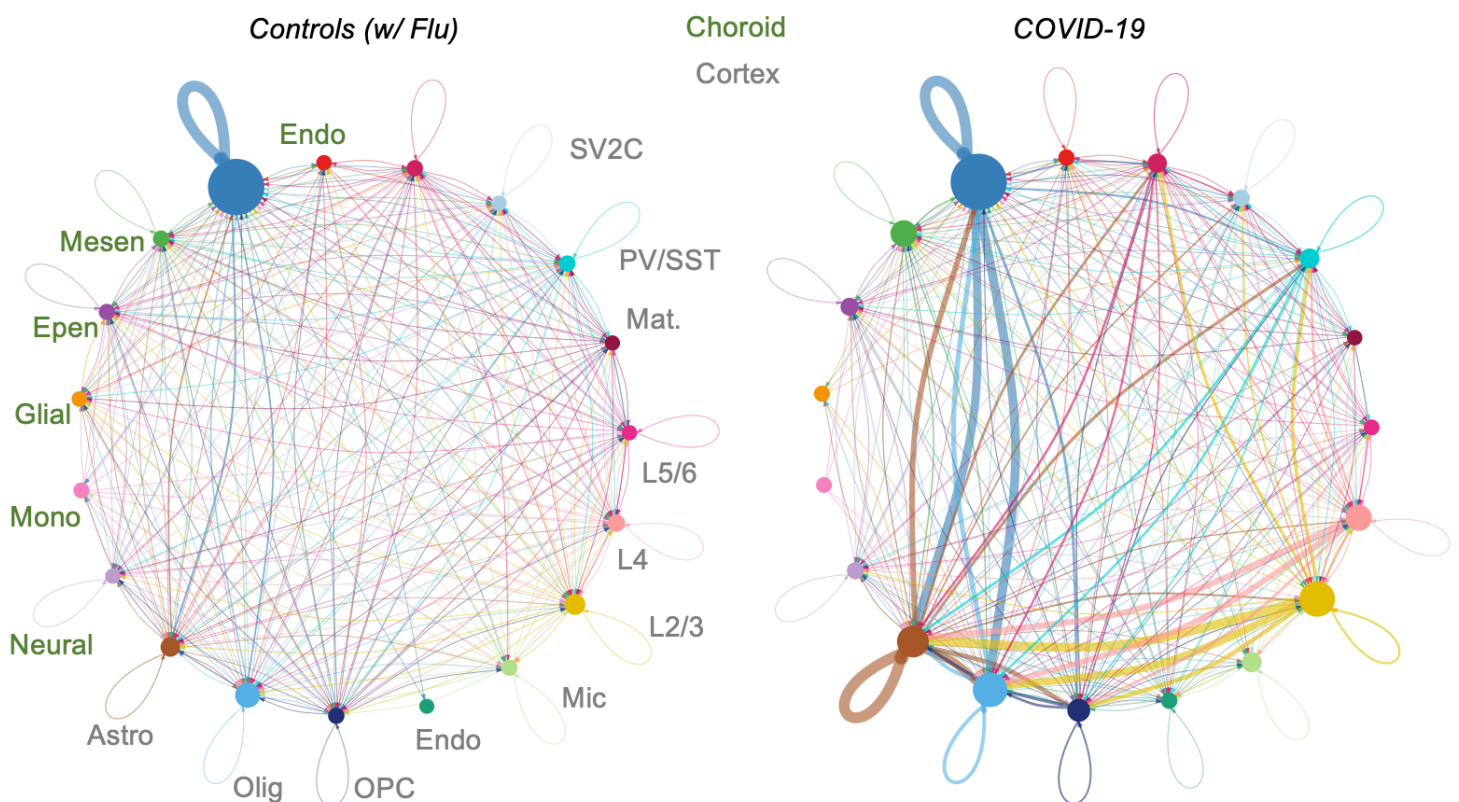
b, Circle plot showing the total inferred intercellular signaling network, aggregating across the signaling molecule interaction (i.e., ligand-receptor) CellChatDB database⁶¹.

Extended Data Figure 5. Cell-type specific changes in gene expression and intercellular signaling in the COVID-19 brain.

a Significantly perturbed pathways in COVID-19



b Increased total intercellular signaling in COVID-19 brains

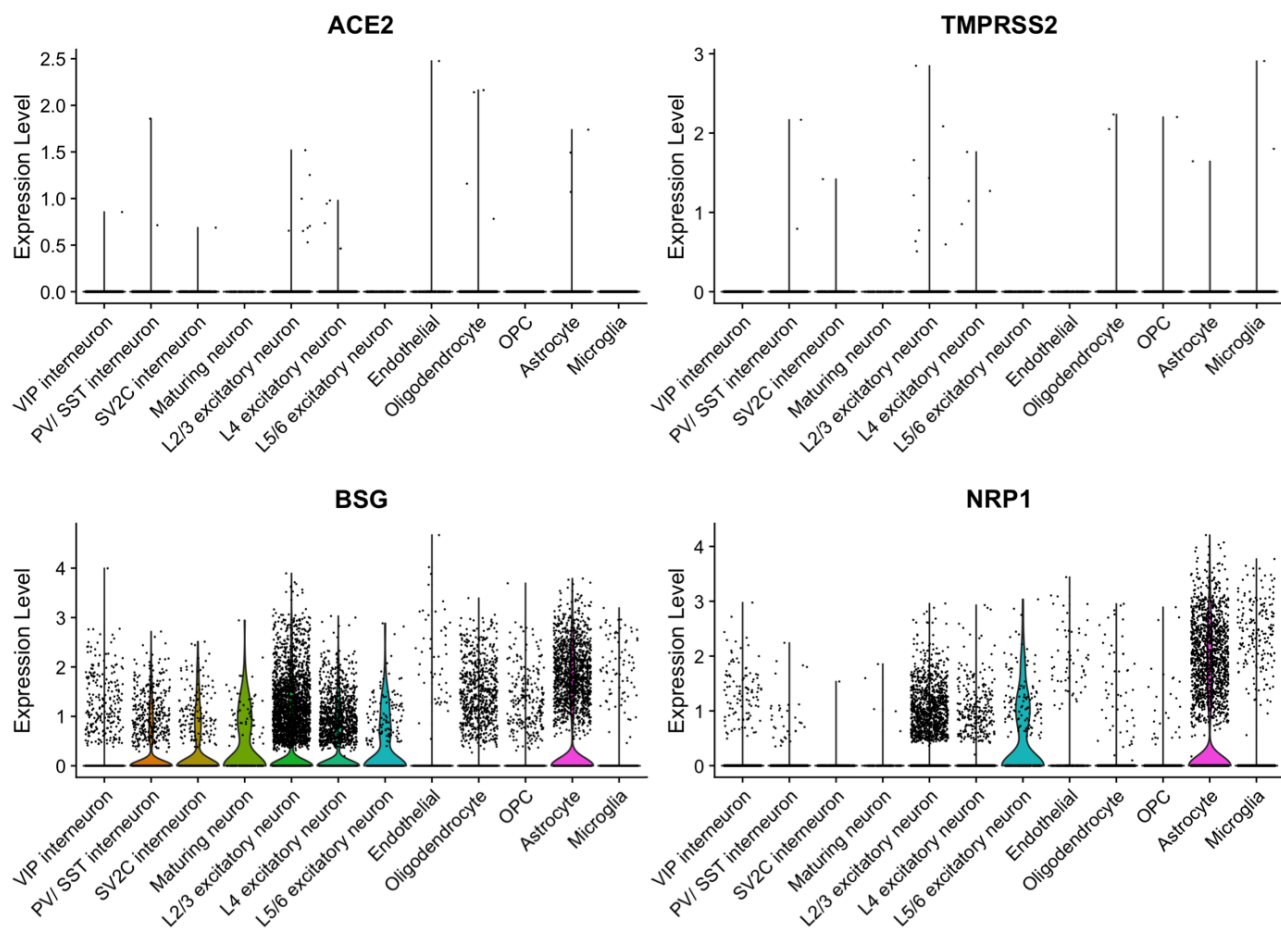


Extended Data Figure 6. Expression of SARS-CoV-2 virus entry genes across cell types.

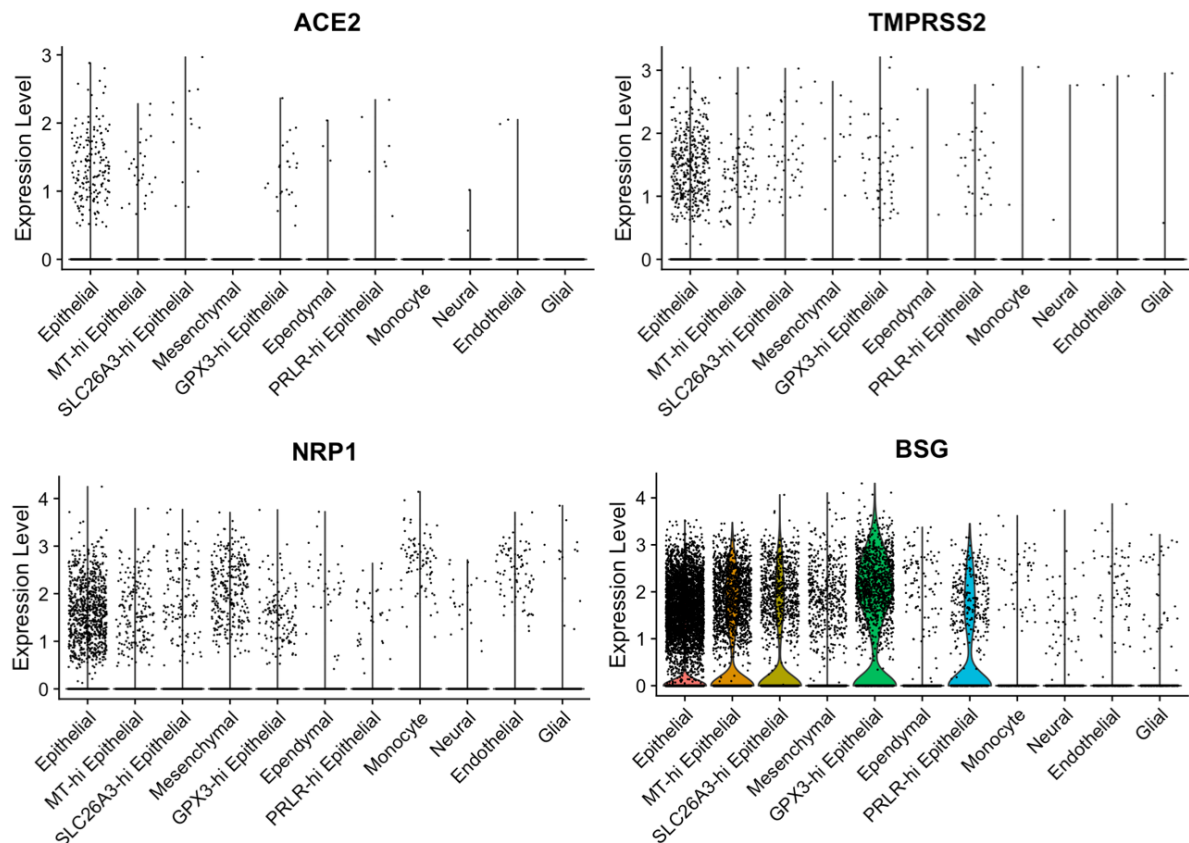
a, b, Expression of SARS-CoV-2 entry receptors, established and putative, across cell types in the human medial frontal cortex (**a**) and choroid plexus (**b**). Violin plots are centered around the median, with their shape representing cell distribution.

Extended Data Figure 6. Expression of SARS-CoV-2 virus entry genes across cell types.

a Frontal medial cortex, parenchymal cells



b Choroid plexus cells



Extended Data Figure 7. Evolution and properties of the COVID-19 enriched microglia cluster.

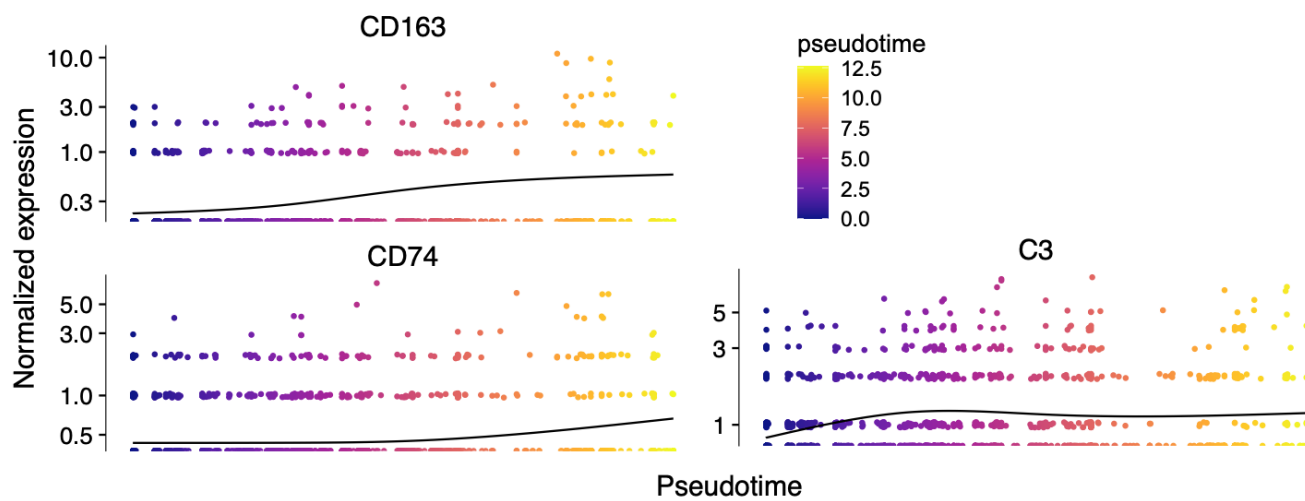
a, b, Expression of established microglia activation markers (**b**) and SARS-CoV-2 entry receptors (**c**) along the pseudotime route in **(a)**. Pseudotime is indicated in graded purple (high) to yellow (high).

c, Overlap (hypergeometric test) between Alzheimer's disease human activated microglia Mic1 marker genes³⁴ and genes upregulated in the COVID-19 enriched Microglia 2 subcluster.

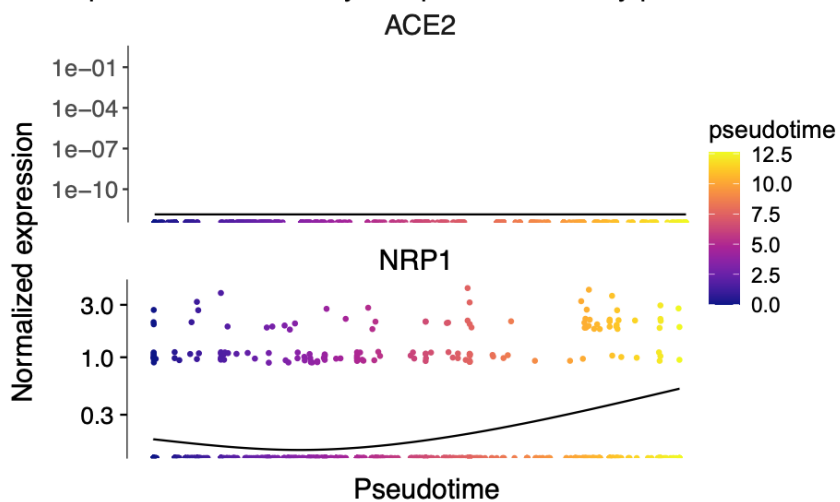
d, Enriched biological pathways amongst Microglia 2 marker genes. Enrichment is based on FDR-corrected cumulative hypergeometric *P* values, with a *P* value-ranked gene-marker list (FDR < 0.01, $\log_2(\text{mean gene expression across Microglia 2} / \text{mean gene expression across all microglia}) > 0.25$, MAST).

Extended Data Figure 7. Evolution and properties of the COVID-19 enriched microglia cluster.

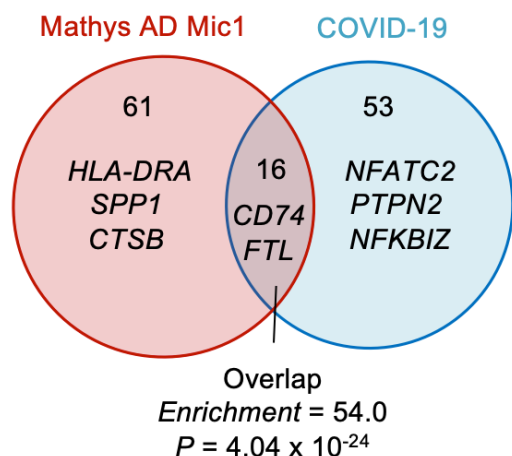
a Expression of microglia activation markers by pseudotime



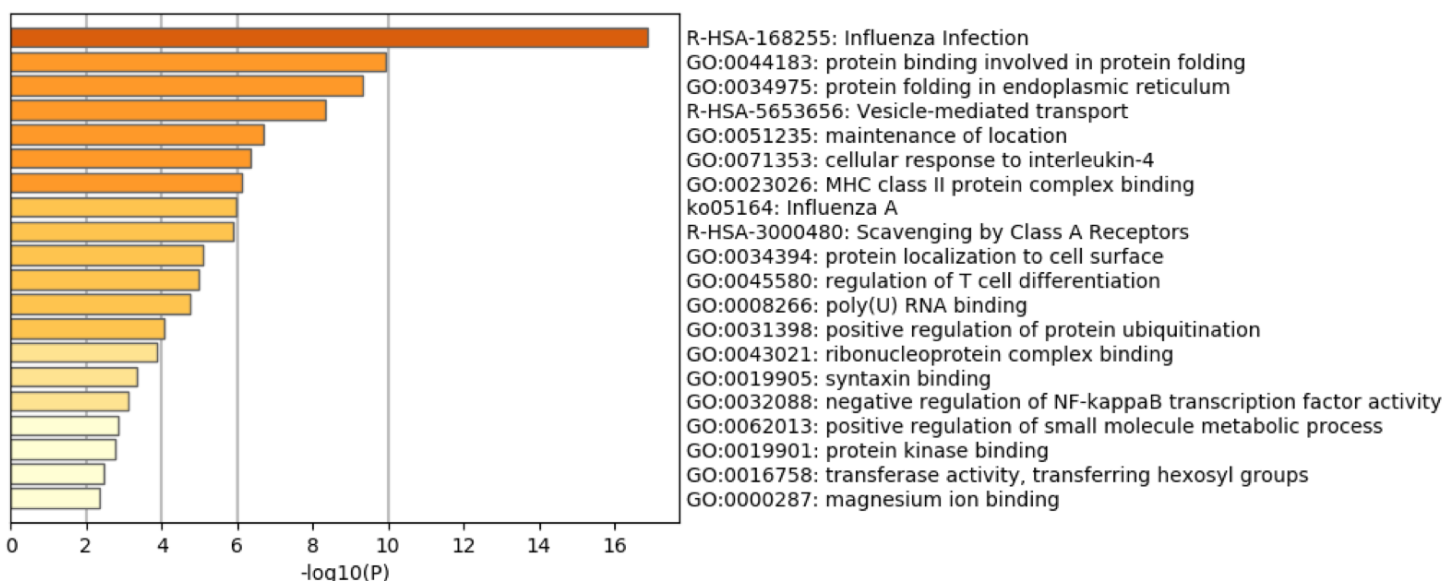
b Expression of viral entry receptors markers by pseudotime



c COVID-19 & AD microglia clusters



d Pathways enriched in COVID-19 microglia 2 cluster (Metascape)



Extended Data Figure 8. Evaluation of COVID-19 enriched subpopulations in other parenchymal glia.

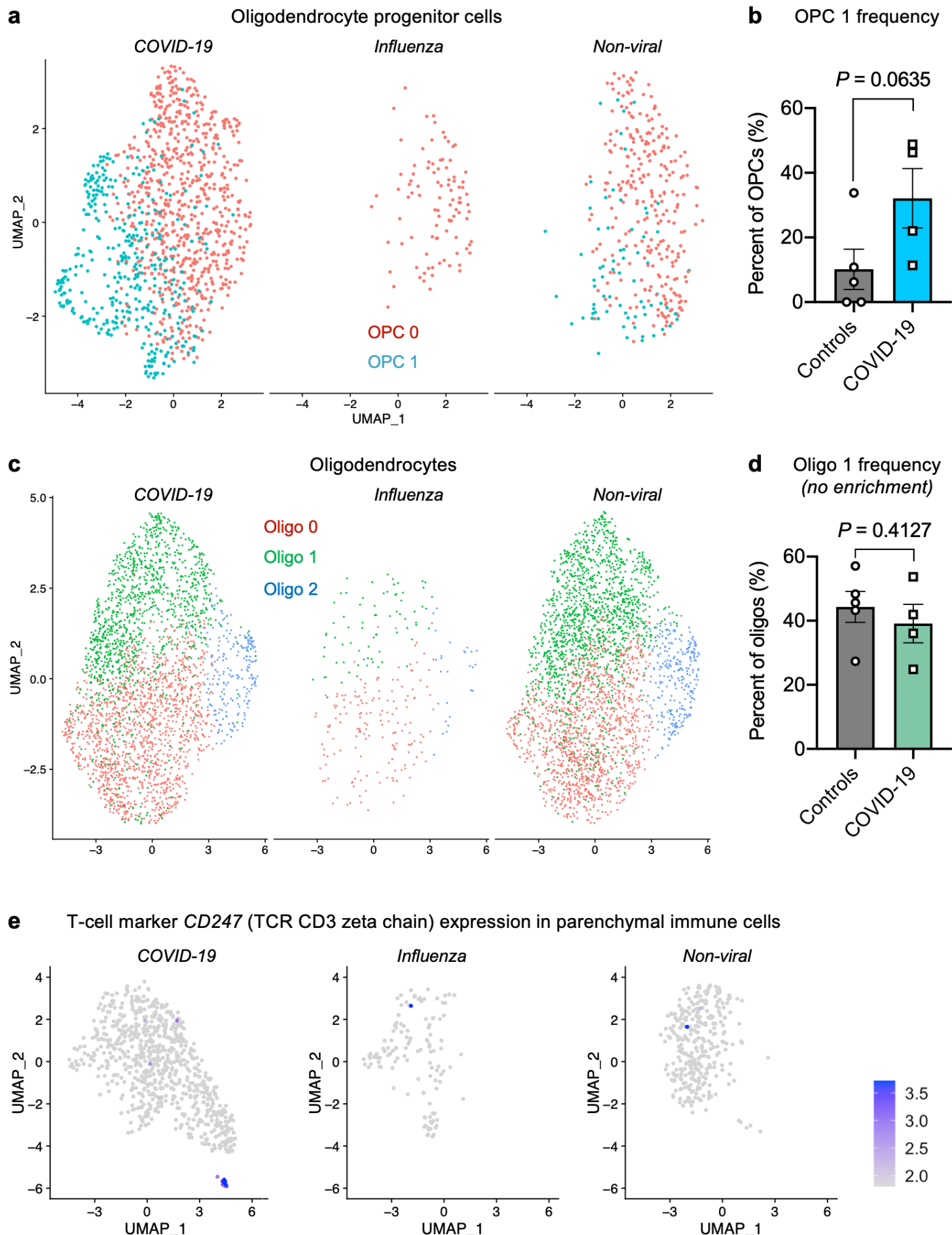
a, UMAP projection of oligodendrocyte progenitor cells (OPCs, $n = 1,634$ from 4 non-viral controls, 1 influenza and 4 COVID-19 individuals) and the emergence of COVID-19 enriched subcluster.

b, Quantification of the frequency of the COVID-19 enriched OPC subcluster as a proportion of all OPCs ($n=5$ controls and $n=4$ COVID-19, two-sided t-test; mean +/- s.e.m.).

c, d, As in **(a-b)** but for oligodendrocytes.

e, Expression of the established T-cell marker *CD247* (encoding TCR CD3 zeta chain) among immune cells captured in human medial frontal cortex.

Extended Data Figure 8. Evaluation of COVID-19 enriched subpopulations in other parenchymal glia



Extended Data Figure 9. Processes downregulated in excitatory neurons in COVID-19.

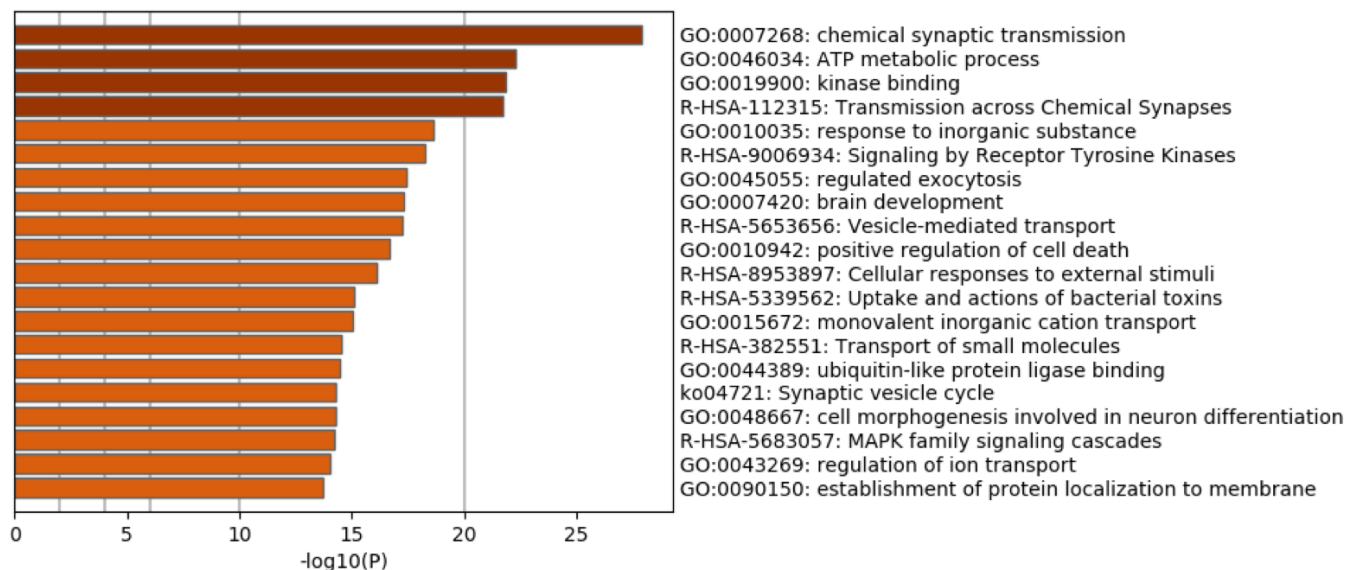
a, Enriched biological pathways amongst downregulated genes in COVID-19 excitatory neurons ($n = 7,680$ from 4 non-viral controls, 1 influenza and 4 COVID-19 individuals). Enrichment is based on FDR-corrected cumulative hypergeometric P values, with a P value-ranked gene-marker list (Log (fold change) > 0.25 (absolute value), adjusted P value (Bonferroni correction) < 0.05 , MAST).

b, As in **(a)** but for Gene Ontology cellular components.

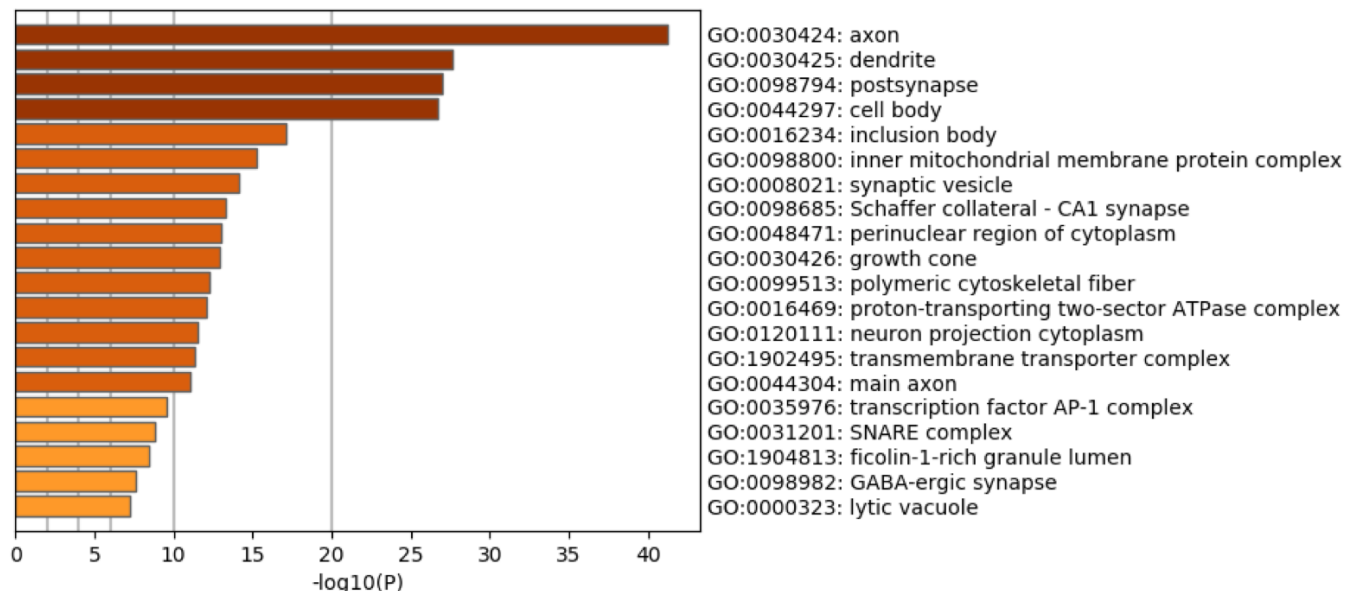
c, As in **(a)** but comparing COVID-19 patients with neurological symptoms versus those without.

Extended Data Figure 9. Processes downregulated in excitatory neurons in COVID-19.

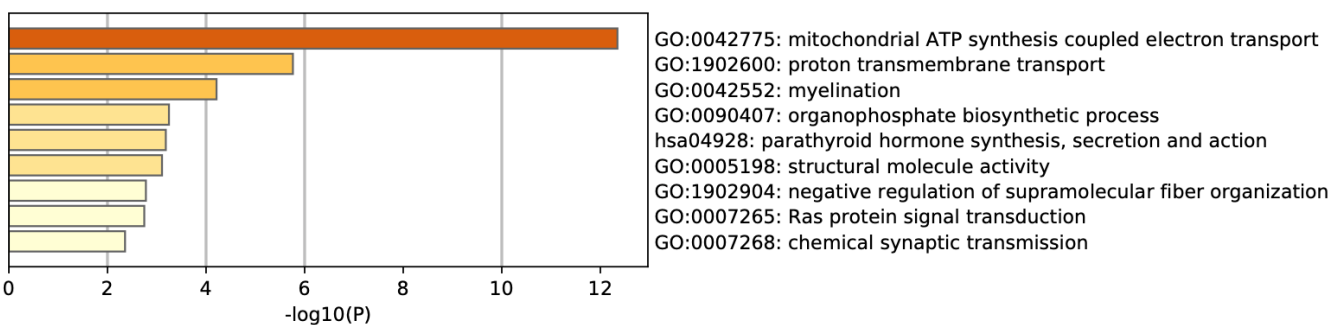
a Biological pathways, downregulated (Metascape)



b Cellular components, downregulated (Metascape)



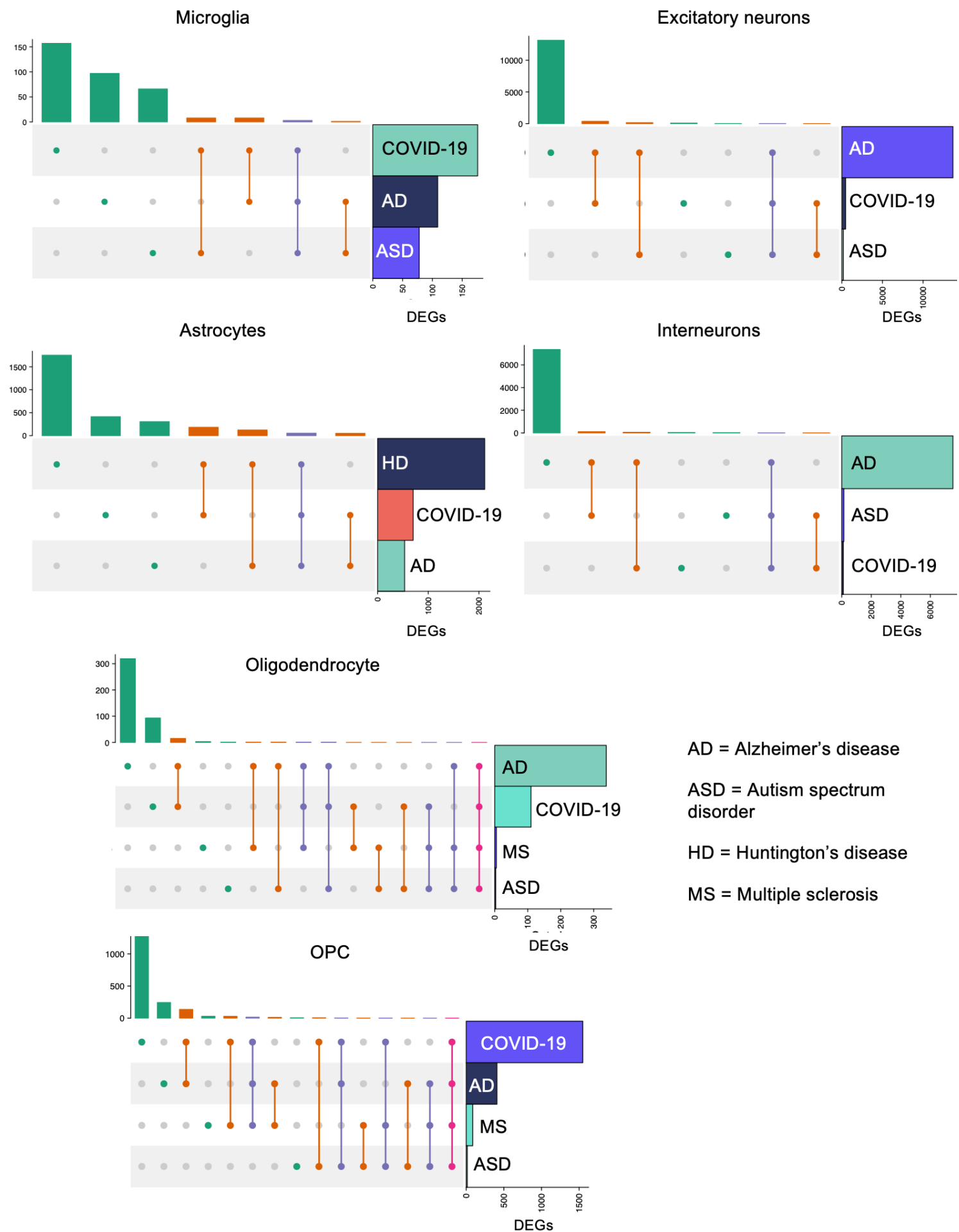
c COVID-19 patients with neurological symptoms versus those without, Pathways downregulated (Metascape)



Extended Data Figure 10. Comparison of cell type-specific changes in COVID-19 with chronic CNS diseases.

Upset matrix plots comparing the cell type-specific genes expression changes in COVID-19 frontal cortex with those previously published for Alzheimer's Disease (AD)³⁴, Autism spectrum disorder (ASD)³³, Huntington's disease (HD)¹²³, and Multiple sclerosis (MS)¹²².

Extended Data Figure 10. Comparison of cell type-specific changes in COVID-19 with chronic CNS diseases.



References

1. Mao, L. *et al.* Neurologic Manifestations of Hospitalized Patients with Coronavirus Disease 2019 in Wuhan, China. *JAMA Neurol.* (2020). doi:10.1001/jamaneurol.2020.1127
2. Yang, X. *et al.* Clinical course and outcomes of critically ill patients with SARS-CoV-2 pneumonia in Wuhan, China: a single-centered, retrospective, observational study. *Lancet Respir. Med.* (2020). doi:10.1016/S2213-2600(20)30079-5
3. Helms, J. *et al.* Neurologic features in severe SARS-COV-2 infection. *New England Journal of Medicine* (2020). doi:10.1056/NEJMc2008597
4. Gidon, A. *et al.* Dendritic action potentials and computation in human layer 2/3 cortical neurons. *Science* (80-). (2020). doi:10.1126/science.aax6239
5. Matschke, J. *et al.* Neuropathology of patients with COVID-19 in Germany: a post-mortem case series. *Lancet Neurol.* (2020).
6. Varatharaj, A. *et al.* Neurological and neuropsychiatric complications of COVID-19 in 153 patients: a UK-wide surveillance study. *The Lancet Psychiatry* (2020). doi:10.1016/S2215-0366(20)30287-X
7. Montalvan, V., Lee, J., Bueso, T., De Toledo, J. & Rivas, K. Neurological manifestations of COVID-19 and other coronavirus infections: A systematic review. *Clinical Neurology and Neurosurgery* (2020). doi:10.1016/j.clineuro.2020.105921
8. Wu, Y. *et al.* Nervous system involvement after infection with COVID-19 and other coronaviruses. *Brain, Behavior, and Immunity* (2020). doi:10.1016/j.bbi.2020.03.031
9. Bialek, S. *et al.* Severe Outcomes Among Patients with Coronavirus Disease 2019 (COVID-19) — United States, February 12–March 16, 2020. *MMWR. Morb. Mortal. Wkly. Rep.* (2020). doi:10.15585/mmwr.mm6912e2
10. Romero-Sánchez, C. M. *et al.* Neurologic manifestations in hospitalized patients with COVID-19: The ALBACOVID registry. *Neurology* (2020). doi:10.1212/WNL.00000000000009937
11. Liotta, E. M. *et al.* Frequent neurologic manifestations and encephalopathy-associated morbidity in Covid-19 patients. *Ann. Clin. Transl. Neurol.* (2020).
12. Rogers, J. P. *et al.* Psychiatric and neuropsychiatric presentations associated with severe coronavirus infections: a systematic review and meta-analysis with comparison to the COVID-19 pandemic. *The Lancet Psychiatry* (2020). doi:10.1016/S2215-0366(20)30203-0
13. Cheng, S. K. W., Wong, C. W., Tsang, J. & Wong, K. C. Psychological distress and negative appraisals in survivors of severe acute respiratory syndrome (SARS). *Psychol. Med.* (2004). doi:10.1017/S0033291704002272
14. Lam, M. H. B. *et al.* Mental morbidities and chronic fatigue in severe acute respiratory syndrome survivors long-term follow-up. *Arch. Intern. Med.* (2009). doi:10.1001/archinternmed.2009.384
15. Ellul, M. A. *et al.* Neurological associations of COVID-19. *The Lancet Neurology* (2020). doi:10.1016/S1474-4422(20)30221-0
16. Iadecola, C., Anrather, J. & Kamel, H. Effects of COVID-19 on the Nervous System. *Cell* (2020). doi:10.1016/j.cell.2020.08.028
17. Puelles, V. G. *et al.* Multiorgan and Renal Tropism of SARS-CoV-2. *The New England journal of medicine* (2020). doi:10.1056/NEJMc2011400
18. Solomon, I. H. *et al.* Neuropathological Features of Covid-19. *The New England journal of medicine* (2020). doi:10.1056/NEJMc2019373
19. Moriguchi, T. *et al.* A first case of meningitis/encephalitis associated with SARS-CoV-2. *Int. J. Infect. Dis.* (2020). doi:10.1016/j.ijid.2020.03.062
20. Meinhardt, J. *et al.* Olfactory transmucosal SARS-CoV-2 invasion as port of Central Nervous System entry in COVID-19 patients. *bioRxiv* (2020).
21. Song, E. *et al.* Neuroinvasive potential of SARS-CoV-2 revealed in a human brain organoid model. *bioRxiv* (2020). doi:10.1101/2020.06.25.169946
22. Ramani, A. *et al.* SARS-CoV-2 targets cortical neurons of 3D human brain organoids and shows neurodegeneration-like effects. *bioRxiv (Preprint)* (2020). doi:10.1101/2020.05.20.106575
23. Pellegrini, L. *et al.* SARS-CoV-2 infects brain choroid plexus and disrupts the blood-CSF-barrier. *bioRxiv* (2020). doi:10.1101/2020.08.20.259937
24. Jacob, F. *et al.* Human Pluripotent Stem Cell-Derived Neural Cells and Brain Organoids Reveal SARS-CoV-2 Neurotropism. *bioRxiv* (2020). doi:10.1101/2020.07.28.225151
25. Zhang, B. Z. *et al.* SARS-CoV-2 infects human neural progenitor cells and brain organoids. *Cell Research* (2020). doi:10.1038/s41422-020-0390-x

26. Mesci, P. *et al.* Sofosbuvir protects human brain organoids against SARS-CoV-2. (2020). doi:10.1101/2020.05.30.125856
27. Bhaduri, A. *et al.* Cell stress in cortical organoids impairs molecular subtype specification. *Nature* (2020). doi:10.1038/s41586-020-1962-0
28. Huch, M., Knoblich, J. A., Lutolf, M. P. & Martinez-Arias, A. The hope and the hype of organoid research. *Dev.* (2017). doi:10.1242/dev.150201
29. Dani, N. *et al.* A cellular and spatial map of the choroid plexus across brain ventricles and ages. *bioRxiv* (2019). doi:10.1101/627539
30. Zhong, S. *et al.* A single-cell RNA-seq survey of the developmental landscape of the human prefrontal cortex. *Nature* (2018). doi:10.1038/nature25980
31. Lake, B. B. *et al.* Integrative single-cell analysis of transcriptional and epigenetic states in the human adult brain. *Nat. Biotechnol.* (2018). doi:10.1038/nbt.4038
32. Grubman, A. *et al.* A single-cell atlas of entorhinal cortex from individuals with Alzheimer's disease reveals cell-type-specific gene expression regulation. *Nat. Neurosci.* (2019). doi:10.1038/s41593-019-0539-4
33. Velmeshev, D. *et al.* Single-cell genomics identifies cell type–specific molecular changes in autism. *Science* (80-). (2019). doi:10.1126/science.aav8130
34. Mathys, H. *et al.* Single-cell transcriptomic analysis of Alzheimer's disease. *Nature* (2019). doi:10.1038/s41586-019-1195-2
35. Zhou, Y. *et al.* Human and mouse single-nucleus transcriptomics reveal TREM2-dependent and TREM2-independent cellular responses in Alzheimer's disease. *Nat. Med.* (2020). doi:10.1038/s41591-019-0695-9
36. Cohen-Cory, S., Kidane, A. H., Shirkey, N. J. & Marshak, S. Brain-derived neurotrophic factor and the development of structural neuronal connectivity. *Developmental Neurobiology* (2010). doi:10.1002/dneu.20774
37. Bathina, S. & Das, U. N. Brain-derived neurotrophic factor and its clinical Implications. *Archives of Medical Science* (2015). doi:10.5114/aoms.2015.56342
38. Prinz, M., Rossum, D. Van & Hanisch, U. K. Interleukin-2 as a Neuroregulatory Cytokine. *NeuroImmune Biology* (2008). doi:10.1016/S1567-7443(07)10008-9
39. Sarder, M., Saito, H. & Abe, K. Interleukin-2 promotes survival and neurite extension of cultured neurons from fetal rat brain. *Brain Res.* (1993). doi:10.1016/0006-8993(93)91080-C
40. Awatsuji, H., Furukawa, Y., Nakajima, M., Furukawa, S. & Hayashi, K. Interleukin-2 as a neurotrophic factor for supporting the survival of neurons cultured from various regions of fetal rat brain. *J. Neurosci. Res.* (1993). doi:10.1002/jnr.490350310
41. Cantuti-Castelvetro, L. *et al.* Neuropilin-1 facilitates SARS-CoV-2 cell entry and provides a possible pathway into the central nervous system. 1–36 (2020). doi:10.1101/2020.06.07.137802
42. Bryce, C. *et al.* Pathophysiology of SARS-CoV-2: targeting of endothelial cells renders a complex disease with thrombotic microangiopathy and aberrant immune response. The Mount Sinai COVID-19 autopsy experience. *medRxiv* (2020).
43. He, L. *et al.* Pericyte-specific vascular expression of SARS-CoV-2 receptor ACE2 – implications for microvascular inflammation and hypercoagulopathy in COVID-19 patients. *bioRxiv* (2020).
44. Shingo, T. *et al.* Pregnancy-stimulated neurogenesis in the adult female forebrain mediated by prolactin. *Science* (80-). (2003). doi:10.1126/science.1076647
45. Larsen, C. M. & Grattan, D. R. Prolactin, neurogenesis, and maternal behaviors. *Brain, Behavior, and Immunity* (2012). doi:10.1016/j.bbi.2011.07.233
46. Saudrais, E., Strazielle, N. & Ghersi-Egea, J. F. Choroid plexus glutathione peroxidases are instrumental in protecting the brain fluid environment from hydroperoxides during postnatal development. *Am. J. Physiol. - Cell Physiol.* (2018). doi:10.1152/ajpcell.00094.2018
47. Saunders, N. R. *et al.* Influx mechanisms in the embryonic and adult rat choroid plexus: A transcriptome study. *Front. Neurosci.* (2015). doi:10.3389/fnins.2015.00123
48. Hodge, R. D. *et al.* Conserved cell types with divergent features in human versus mouse cortex. *Nature* (2019). doi:10.1038/s41586-019-1506-7
49. Bailey, C. C., Zhong, G., Huang, I. C. & Farzan, M. IFITM-family proteins: The cell's first line of antiviral defense. *Annu. Rev. Virol.* (2014). doi:10.1146/annurev-virology-031413-085537
50. Hachim, M. Y. *et al.* Interferon-Induced Transmembrane Protein (IFITM3) Is Upregulated Explicitly in SARS-CoV-2 Infected Lung Epithelial Cells. *Front. Immunol.* (2020).

- doi:10.3389/fimmu.2020.01372
- 51. Daly, J. L. *et al.* Neuropilin-1 is a host factor for SARS-CoV-2 infection. *bioRxiv* (2020).
 - 52. Moutal, A. *et al.* SARS-CoV-2 Spike protein co-opts VEGF-A/Neuropilin-1 receptor signaling to induce analgesia. *Pain* (2020). doi:10.1097/j.pain.0000000000002097
 - 53. Ackermann, M. *et al.* Pulmonary vascular endothelialitis, thrombosis, and angiogenesis in Covid-19. *N. Engl. J. Med.* (2020). doi:10.1056/NEJMoa2015432
 - 54. Shaftel, S. S. *et al.* Sustained hippocampal IL-1 β overexpression mediates chronic neuroinflammation and ameliorates Alzheimer plaque pathology. *J. Clin. Invest.* (2007). doi:10.1172/JCI31450
 - 55. Shaftel, S. S. *et al.* Chronic interleukin-1 β expression in mouse brain leads to leukocyte infiltration and neutrophil-independent blood-brain barrier permeability without overt neurodegeneration. *J. Neurosci.* (2007). doi:10.1523/JNEUROSCI.1418-07.2007
 - 56. Mahad, D. *et al.* Modulating CCR2 and CCL2 at the blood-brain barrier: Relevance for multiple sclerosis pathogenesis. *Brain* (2006). doi:10.1093/brain/awh655
 - 57. Guedes, J. R., Lao, T., Cardoso, A. L. & El Khoury, J. Roles of microglial and monocyte chemokines and their receptors in regulating Alzheimer's disease-associated amyloid- β and tau pathologies. *Frontiers in Neurology* (2018). doi:10.3389/fneur.2018.00549
 - 58. Cui, J. *et al.* Inflammation of the embryonic blood-cerebrospinal fluid barrier following maternal immune activation. *Submitt. to Dev Cell* 1–12 (2020). doi:10.1016/j.devcel.2020.09.020
 - 59. Baruch, K. *et al.* Aging-induced type I interferon response at the choroid plexus negatively affects brain function. *Science* (80-.). (2014). doi:10.1126/science.1252945
 - 60. Baruch, K. *et al.* CNS-specific immunity at the choroid plexus shifts toward destructive Th2 inflammation in brain aging. *Proc. Natl. Acad. Sci. U. S. A.* (2013). doi:10.1073/pnas.1211270110
 - 61. Jin, S., Guerrero-juarez, C. F., Zhang, L., Chang, I. & Myung, P. Inference and analysis of cell-cell communication using CellChat. *bioRxiv* (2020).
 - 62. Efremova, M., Vento-Tormo, M., Teichmann, S. A. & Vento-Tormo, R. CellPhoneDB: inferring cell–cell communication from combined expression of multi-subunit ligand–receptor complexes. *Nat. Protoc.* (2020). doi:10.1038/s41596-020-0292-x
 - 63. Thrupp, N. *et al.* Single-Nucleus RNA-Seq Is Not Suitable for Detection of Microglial Activation Genes in Humans. *Cell Rep.* (2020). doi:10.1016/j.celrep.2020.108189
 - 64. Trapnell, C. *et al.* The dynamics and regulators of cell fate decisions are revealed by pseudotemporal ordering of single cells. *Nat. Biotechnol.* (2014). doi:10.1038/nbt.2859
 - 65. Hammond, T. R. *et al.* Single-Cell RNA Sequencing of Microglia throughout the Mouse Lifespan and in the Injured Brain Reveals Complex Cell-State Changes. *Immunity* (2019). doi:10.1016/j.jimmuni.2018.11.004
 - 66. Cochain, C. *et al.* Single-cell RNA-seq reveals the transcriptional landscape and heterogeneity of aortic macrophages in murine atherosclerosis. *Circ. Res.* (2018). doi:10.1161/CIRCRESAHA.117.312509
 - 67. Bryan, K. J. *et al.* Expression of CD74 is increased in neurofibrillary tangles in Alzheimer's disease. *Mol. Neurodegener.* (2008). doi:10.1186/1750-1326-3-13
 - 68. Borghese, F. & Clanchy, F. II. CD74: An emerging opportunity as a therapeutic target in cancer and autoimmune disease. *Expert Opinion on Therapeutic Targets* (2011). doi:10.1517/14728222.2011.550879
 - 69. Mathys, H. *et al.* Temporal Tracking of Microglia Activation in Neurodegeneration at Single-Cell Resolution. *Cell Rep.* (2017). doi:10.1016/j.celrep.2017.09.039
 - 70. Hoperton, K. E., Mohammad, D., Trépanier, M. O., Giuliano, V. & Bazinet, R. P. Markers of microglia in post-mortem brain samples from patients with Alzheimer's disease: A systematic review. *Molecular Psychiatry* (2018). doi:10.1038/mp.2017.246
 - 71. Nomura, K., Vilalta, A., Allendorf, D. H., Hornik, T. C. & Brown, G. C. Activated Microglia Desialylate and Phagocytose Cells via Neuraminidase, Galectin-3, and Mer Tyrosine Kinase. *J. Immunol.* (2017). doi:10.4049/jimmunol.1502532
 - 72. Healy, L. M. *et al.* MerTK Is a Functional Regulator of Myelin Phagocytosis by Human Myeloid Cells. *J. Immunol.* (2016). doi:10.4049/jimmunol.1502562
 - 73. Lew, D. S., Mazzoni, F. & Finnemann, S. C. Microglia Inhibition Delays Retinal Degeneration Due to MerTK Phagocytosis Receptor Deficiency. *Front. Immunol.* (2020). doi:10.3389/fimmu.2020.01463

74. Tondo, G., Perani, D. & Comi, C. TAM receptor pathways at the crossroads of neuroinflammation and neurodegeneration. *Disease Markers* (2019). doi:10.1155/2019/2387614
75. Kobayashi, K. et al. IRAK-M is a negative regulator of Toll-like receptor signaling. *Cell* (2002). doi:10.1016/S0092-8674(02)00827-9
76. Lyu, C. et al. IRAK-M deficiency exacerbates ischemic neurovascular injuries in experimental stroke mice. *Front. Cell. Neurosci.* (2018). doi:10.3389/fncel.2018.00504
77. Deczkowska, A. et al. Mef2C restrains microglial inflammatory response and is lost in brain ageing in an IFN-I-dependent manner. *Nat. Commun.* (2017). doi:10.1038/s41467-017-00769-0
78. Hong, S. et al. Complement and microglia mediate early synapse loss in Alzheimer mouse models. *Science* (80-). (2016). doi:10.1126/science.aad8373
79. Stevens, B. et al. The Classical Complement Cascade Mediates CNS Synapse Elimination. *Cell* (2007). doi:10.1016/j.cell.2007.10.036
80. Lehrman, E. K. et al. CD47 Protects Synapses from Excess Microglia-Mediated Pruning during Development. *Neuron* (2018). doi:10.1016/j.neuron.2018.09.017
81. Brown, G. C. & Neher, J. J. Microglial phagocytosis of live neurons. *Nat. Rev. Neurosci.* (2014). doi:10.1038/nrn3710
82. Sofroniew, M. V. Astrocyte barriers to neurotoxic inflammation. *Nature Reviews Neuroscience* (2015). doi:10.1038/nrn3898
83. Owens, T., Bechmann, I. & Engelhardt, B. Perivascular spaces and the two steps to neuroinflammation. *Journal of Neuropathology and Experimental Neurology* (2008). doi:10.1097/NEN.0b013e31818f9ca8
84. Allen, N. J. & Eroglu, C. Cell Biology of Astrocyte-Synapse Interactions. *Neuron* (2017). doi:10.1016/j.neuron.2017.09.056
85. Chung, W. S., Allen, N. J. & Eroglu, C. Astrocytes control synapse formation, function, and elimination. *Cold Spring Harb. Perspect. Biol.* (2015). doi:10.1101/cshperspect.a020370
86. Perea, G., Navarrete, M. & Araque, A. Tripartite synapses: astrocytes process and control synaptic information. *Trends in Neurosciences* (2009). doi:10.1016/j.tins.2009.05.001
87. Eng, L. F. & Ghirnikar, R. S. GFAP and Astrogliosis. in *Brain Pathology* (1994). doi:10.1111/j.1750-3639.1994.tb00838.x
88. Llorens, F. et al. YKL-40 in the brain and cerebrospinal fluid of neurodegenerative dementias. *Mol. Neurodegener.* (2017). doi:10.1186/s13024-017-0226-4
89. Matute-Blanch, C. et al. Chitinase 3-like 1 is neurotoxic in primary cultured neurons. *Sci. Rep.* (2020). doi:10.1038/s41598-020-64093-2
90. Moreno-Rodriguez, M., Perez, S. E., Nadeem, M., Malek-Ahmadi, M. & Mufson, E. J. Frontal cortex chitinase and pentraxin neuroinflammatory alterations during the progression of Alzheimer's disease. *J. Neuroinflammation* (2020). doi:10.1186/s12974-020-1723-x
91. Kim, K. et al. Role of Excitatory Amino Acid Transporter-2 (EAAT2) and glutamate in neurodegeneration: Opportunities for developing novel therapeutics. *Journal of Cellular Physiology* (2011). doi:10.1002/jcp.22609
92. Su, Z. zhong et al. Insights into glutamate transport regulation in human astrocytes: Cloning of the promoter for excitatory amino acid transporter 2 (EAAT2). *Proc. Natl. Acad. Sci. U. S. A.* (2003). doi:10.1073/pnas.0136555100
93. Maragakis, N. J., Dykes-Hoberg, M. & Rothstein, J. D. Altered Expression of the Glutamate Transporter EAAT2b in Neurological Disease. *Ann. Neurol.* (2004). doi:10.1002/ana.20003
94. Lewerenz, J. & Maher, P. Chronic glutamate toxicity in neurodegenerative diseases-What is the evidence? *Frontiers in Neuroscience* (2015). doi:10.3389/fnins.2015.00469
95. Dong, X. X., Wang, Y. & Qin, Z. H. Molecular mechanisms of excitotoxicity and their relevance to pathogenesis of neurodegenerative diseases. *Acta Pharmacologica Sinica* (2009). doi:10.1038/aps.2009.24
96. Kullmann, D. M. & Asztely, F. Extrasynaptic glutamate spillover in the hippocampus: Evidence and implications. *Trends Neurosci.* (1998). doi:10.1016/S0166-2236(97)01150-8
97. Diamond, J. S. A broad view of glutamate spillover. *Nature Neuroscience* (2002). doi:10.1038/nrn0402-291
98. Rose, C. R. et al. Astroglial glutamate signaling and uptake in the hippocampus. *Frontiers in Molecular Neuroscience* (2018). doi:10.3389/fnmol.2017.00451
99. Filosa, A. et al. Neuron-glia communication via EphA4/ephrin-A3 modulates LTP through glial

- glutamate transport. *Nat. Neurosci.* (2009). doi:10.1038/nn.2394
100. Robinson, M. B. & Jackson, J. G. Astroglial glutamate transporters coordinate excitatory signaling and brain energetics. *Neurochemistry International* (2016). doi:10.1016/j.neuint.2016.03.014
101. Carmona, M. A., Murai, K. K., Wang, L., Roberts, A. J. & Pasqualea, E. B. Glial ephrin-A3 regulates hippocampal dendritic spine morphology and glutamate transport. *Proc. Natl. Acad. Sci. U. S. A.* (2009). doi:10.1073/pnas.0903328106
102. Ohno, Y., Kinboshi, M. & Shimizu, S. Inwardly rectifying potassium channel kir4.1 as a novel modulator of BDNF expression in astrocytes. *International Journal of Molecular Sciences* (2018). doi:10.3390/ijms19113313
103. Ramakrishnan, N. A., Drescher, M. J. & Drescher, D. G. The SNARE complex in neuronal and sensory cells. *Molecular and Cellular Neuroscience* (2012). doi:10.1016/j.mcn.2012.03.009
104. Südhof, T. C. & Malenka, R. C. Understanding Synapses: Past, Present, and Future. *Neuron* (2008). doi:10.1016/j.neuron.2008.10.011
105. Davison, A. Basic Neurochemistry: Molecular, Cellular, and Medical Aspects. *J. Neurol. Neurosurg. Psychiatry* (1989). doi:10.1136/jnnp.52.8.1021-a
106. Hess, E. J., Jinnah, H. A., Kozak, C. A. & Wilson, M. C. Spontaneous locomotor hyperactivity in a mouse mutant with a deletion including the Snap gene on chromosome 2. *J. Neurosci.* (1992). doi:10.1523/jneurosci.12-07-02865.1992
107. Thompson, P. M., Sower, A. C. & Perrone-Bizzozero, N. I. Altered levels of the synaptosomal associated protein SNAP-25 in schizophrenia. *Biol. Psychiatry* (1998). doi:10.1016/S0006-3223(97)00204-7
108. Gabriel, S. M. et al. Increased concentrations of presynaptic proteins in the cingulate cortex of subjects with schizophrenia. *Arch. Gen. Psychiatry* (1997). doi:10.1001/archpsyc.1997.01830180077010
109. Berchtold, N. C. et al. Synaptic genes are extensively downregulated across multiple brain regions in normal human aging and Alzheimer's disease. *Neurobiol. Aging* (2013). doi:10.1016/j.neurobiolaging.2012.11.024
110. Vardar, G. et al. Distinct functions of syntaxin-1 in neuronal maintenance, synaptic vesicle docking, and fusion in mouse neurons. *J. Neurosci.* (2016). doi:10.1523/JNEUROSCI.1314-16.2016
111. Arancillo, M. et al. Titration of Syntaxin1 in mammalian synapses reveals multiple roles in vesicle docking, priming, and release probability. *J. Neurosci.* (2013). doi:10.1523/JNEUROSCI.0187-13.2013
112. Yang, H. et al. Brain-Specific SNAP-25 Deletion Leads to Elevated Extracellular Glutamate Level and Schizophrenia-Like Behavior in Mice. *Neural Plast.* (2017). doi:10.1155/2017/4526417
113. Sharma, M. et al. CSP α knockout causes neurodegeneration by impairing SNAP-25 function. *EMBO J.* (2012). doi:10.1038/embj.2011.467
114. Vuong, C. K. et al. Rbfox1 Regulates Synaptic Transmission through the Inhibitory Neuron-Specific vSNARE Vamp1. *Neuron* (2018). doi:10.1016/j.neuron.2018.03.008
115. Schoch, S. et al. SNARE function analyzed in synaptobrevin/VAMP knockout mice. *Science* (80-). (2001). doi:10.1126/science.1064335
116. Blasi, J. et al. Inhibition of neurotransmitter release by clostridial neurotoxins correlates with specific proteolysis of synaptosomal proteins. *J. Physiol. - Paris* (1994). doi:10.1016/0928-4257(94)90086-8
117. Wang, D. et al. Syntaxin requirement for Ca²⁺-triggered exocytosis in neurons and endocrine cells demonstrated with an engineered neurotoxin. *Biochemistry* (2011). doi:10.1021/bi200290p
118. Washbourne, P. et al. Genetic ablation of the t-SNARE SNAP-25 distinguishes mechanisms of neuroexocytosis. *Nat. Neurosci.* (2002). doi:10.1038/nn783
119. Feldmeyer, D. Excitatory neuronal connectivity in the barrel cortex. *Front. Neuroanat.* (2012). doi:10.3389/fnana.2012.00024
120. Petersen, C. C. H. & Crochet, S. Synaptic Computation and Sensory Processing in Neocortical Layer 2/3. *Neuron* (2013). doi:10.1016/j.neuron.2013.03.020
121. Marshall, M. How COVID-19 can damage the brain. *Nature* (2020). doi:10.1038/d41586-020-02599-5
122. Jäkel, S. et al. Altered human oligodendrocyte heterogeneity in multiple sclerosis. *Nature* (2019). doi:10.1038/s41586-019-0903-2

123. Al-Dalahmah, O. *et al.* Single-nucleus RNA-seq identifies Huntington disease astrocyte states. *Acta Neuropathol. Commun.* (2020). doi:10.1186/s40478-020-0880-6
124. Maurano, M. T. *et al.* Systematic localization of common disease-associated variation in regulatory DNA. *Science* (80-.). (2012). doi:10.1126/science.1222794
125. Nott, A. *et al.* Brain cell type–specific enhancer–promoter interactome maps and disease-risk association. *Science* (80-.). (2019). doi:10.1126/science.aay0793
126. Buniello, A. *et al.* The NHGRI-EBI GWAS Catalog of published genome-wide association studies, targeted arrays and summary statistics 2019. *Nucleic Acids Res.* (2019). doi:10.1093/nar/gky1120
127. Wang, D. *et al.* Comprehensive functional genomic resource and integrative model for the human brain. *Science* (80-.). (2018). doi:10.1126/science.aat8464
128. Lewis, D. A. The chandelier neuron in schizophrenia. *Dev. Neurobiol.* (2011). doi:10.1002/dneu.20825
129. Pierri, J. N., Volk, C. L. E., Auh, S., Sampson, A. & Lewis, D. A. Decreased somal size of deep layer 3 pyramidal neurons in the prefrontal cortex of subjects with schizophrenia. *Arch. Gen. Psychiatry* (2001). doi:10.1001/archpsyc.58.5.466
130. Garey, L. When cortical development goes wrong: Schizophrenia as a neurodevelopmental disease of microcircuits. *J. Anat.* (2010). doi:10.1111/j.1469-7580.2010.01231.x
131. Shrestha, P., Mousa, A. & Heintz, N. Layer 2/3 pyramidal cells in the medial prefrontal cortex moderate stress induced depressive behaviors. *eLife* (2015). doi:10.7554/eLife.08752
132. Granato, A. & De Giorgio, A. Alterations of neocortical pyramidal neurons: Turning points in the genesis of mental retardation. *Frontiers in Pediatrics* (2014). doi:10.3389/fped.2014.00086
133. Zhou, X. *et al.* Astrocyte, a promising target for mood disorder interventions. *Frontiers in Molecular Neuroscience* (2019). doi:10.3389/fnmol.2019.00136
134. Rajkowska, G. & Stockmeier, C. Astrocyte Pathology in Major Depressive Disorder: Insights from Human Postmortem Brain Tissue. *Curr. Drug Targets* (2013). doi:10.2174/13894501113149990156
135. Tarasov, V. V. *et al.* Alterations of astrocytes in the context of schizophrenic dementia. *Frontiers in Pharmacology* (2020). doi:10.3389/fphar.2019.01612
136. Swain, A., Bhagat, H., Sahni, N. & Salunke, P. Mechanical ventilation in neurological and neurosurgical patients. *Neurol. India* (2016). doi:10.4103/0028-3886.181585
137. Hosseini, S. *et al.* Long-term neuroinflammation induced by influenza a virus infection and the impact on hippocampal neuron morphology and function. *J. Neurosci.* (2018). doi:10.1523/JNEUROSCI.1740-17.2018
138. Casals, J., Elizan, T. S. & Yahr, M. D. Postencephalitic parkinsonism - A review. *Journal of Neural Transmission* (1998). doi:10.1007/s007020050086
139. Readhead, B. *et al.* Multiscale Analysis of Independent Alzheimer's Cohorts Finds Disruption of Molecular, Genetic, and Clinical Networks by Human Herpesvirus. *Neuron* (2018). doi:10.1016/j.neuron.2018.05.023
140. Deleidi, M. & Isaacson, O. Viral and inflammatory triggers of neurodegenerative diseases. *Science Translational Medicine* (2012). doi:10.1126/scitranslmed.3003492
141. Yousef, H. *et al.* Aged blood impairs hippocampal neural precursor activity and activates microglia via brain endothelial cell VCAM1. *Nat. Med.* (2019). doi:10.1038/s41591-019-0440-4
142. Chen, M. B. *et al.* Brain Endothelial Cells Are Exquisite Sensors of Age-Related Circulatory Cues. *Cell Rep.* (2020). doi:10.1016/j.celrep.2020.03.012
143. Petersen, M. A., Ryu, J. K. & Akassoglou, K. Fibrinogen in neurological diseases: Mechanisms, imaging and therapeutics. *Nature Reviews Neuroscience* (2018). doi:10.1038/nrn.2018.13
144. Yang, A. C. *et al.* Physiological blood–brain transport is impaired with age by a shift in transcytosis. *Nature* (2020). doi:10.1038/s41586-020-2453-z
145. Garrigues, E. *et al.* Post-discharge persistent symptoms and health-related quality of life after hospitalization for COVID-19. *Journal of Infection* (2020). doi:10.1016/j.jinf.2020.08.029
146. Kaseda, E. T. & Levine, A. J. Post-traumatic stress disorder: a differential diagnostic consideration for COVID-19 survivors. *Clinical Neuropsychologist* (2020). doi:10.1080/13854046.2020.1811894
147. Vallejo-Illarramendi, A., Torres-Ramos, M., Melone, M., Conti, F. & Matute, C. Clozapine reduces GLT-1 expression and glutamate uptake in astrocyte cultures. *Glia* (2005). doi:10.1002/glia.20172
148. Swiech, L. *et al.* In vivo interrogation of gene function in the mammalian brain using CRISPR-Cas9. *Nat. Biotechnol.* (2015). doi:10.1038/nbt.3055

149. Corces, M. R. *et al.* An improved ATAC-seq protocol reduces background and enables interrogation of frozen tissues. *Nat. Methods* (2017). doi:10.1038/nmeth.4396
150. McInnes, L., Healy, J., Saul, N. & Großberger, L. UMAP: Uniform Manifold Approximation and Projection. *J. Open Source Softw.* (2018). doi:10.21105/joss.00861
151. Young, M. & Behjati, S. SoupX removes ambient RNA contamination from droplet based single-cell RNA sequencing data. *bioRxiv* (2018). doi:10.1101/303727
152. Satija, R., Farrell, J. A., Gennert, D., Schier, A. F. & Regev, A. Spatial reconstruction of single-cell gene expression data. *Nat. Biotechnol.* (2015). doi:10.1038/nbt.3192
153. McGinnis, C. S., Murrow, L. M. & Garther, Z. J. DoubletFinder: Doublet Detection in Single-Cell RNA Sequencing Data Using Artificial Nearest Neighbors. *Cell Syst.* (2019). doi:10.1016/j.cels.2019.03.003
154. Finak, G. *et al.* MAST: A flexible statistical framework for assessing transcriptional changes and characterizing heterogeneity in single-cell RNA sequencing data. *Genome Biol.* (2015). doi:10.1186/s13059-015-0844-5
155. Chen, E. Y. *et al.* Enrichr: Interactive and collaborative HTML5 gene list enrichment analysis tool. *BMC Bioinformatics* (2013). doi:10.1186/1471-2105-14-128
156. Zhou, Y. *et al.* Metascape provides a biologist-oriented resource for the analysis of systems-level datasets. *Nat. Commun.* (2019). doi:10.1038/s41467-019-09234-6
157. Gerstner, N. *et al.* GeneTrail 3: advanced high-throughput enrichment analysis. *Nucleic Acids Res.* (2020). doi:10.1093/nar/gkaa306
158. Bost, P. *et al.* Host-Viral Infection Maps Reveal Signatures of Severe COVID-19 Patients. *Cell* (2020). doi:10.1016/j.cell.2020.05.006
159. Kim, D., Song, L., Breitwieser, F. P. & Salzberg, S. L. Centrifuge: Rapid and sensitive classification of metagenomic sequences. *Genome Res.* (2016). doi:10.1101/gr.210641.116
160. Stano, M., Beke, G. & Klucar, L. ViruSITE - Integrated database for viral genomics. *Database* (2016). doi:10.1093/database/baw162
161. Wauters, E. *et al.* Discriminating Mild from Critical COVID-19 by Innate and Adaptive Immune Single-cell Profiling of Bronchoalveolar Lavages. (2020). doi:10.1101/2020.07.09.196519